

AD-A039 161

AIR FORCE INST OF TECH WRIGHT-PATTERSON AFB OHIO SCH--ETC F/G 21/5  
AN INVESTIGATION OF LASER-TARGET INTERACTION SIGNALS.(U)

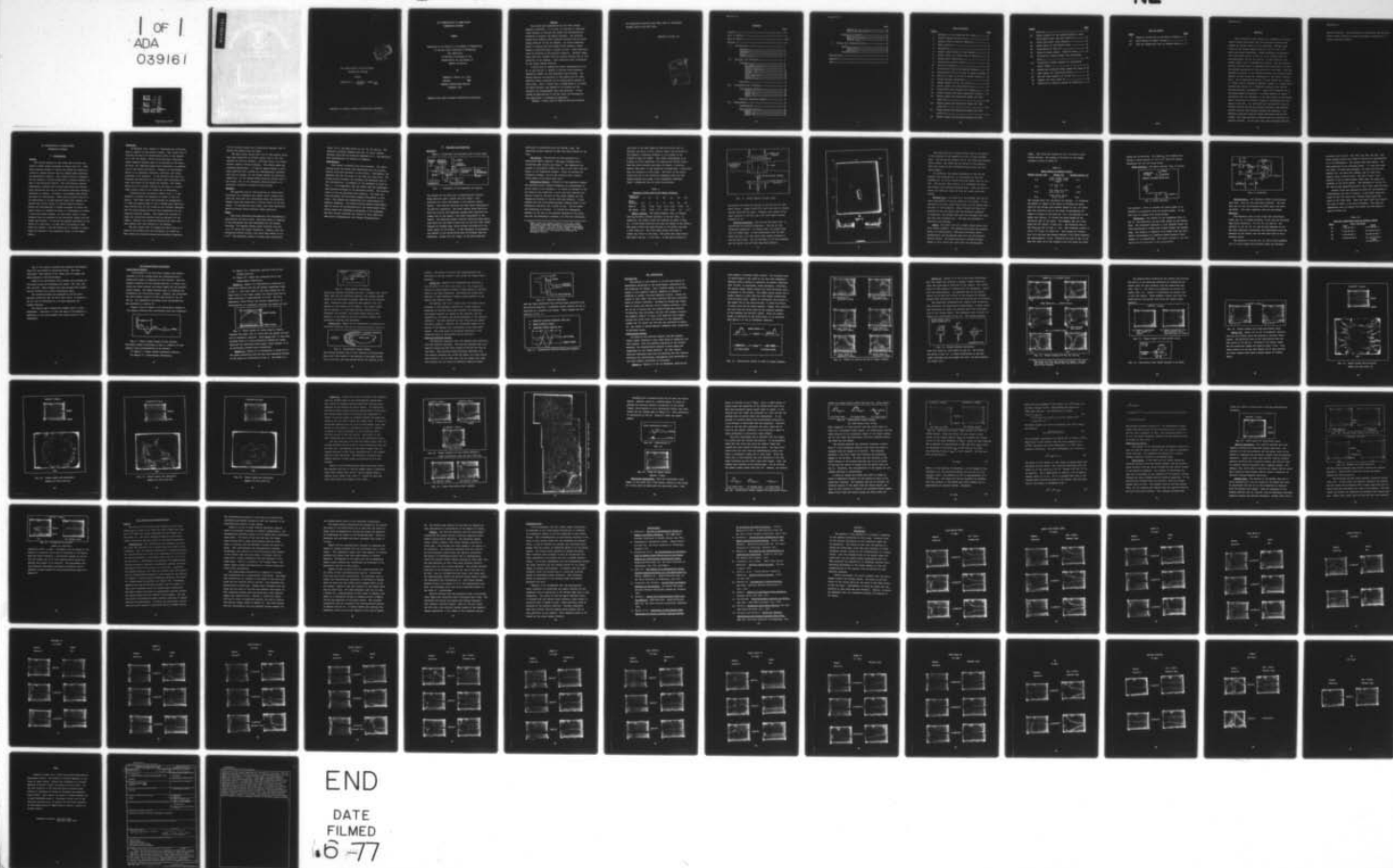
DEC 75 R D ARLEN

AFIT/GEP/PH/75D-14

UNCLASSIFIED

NL

1 OF 1  
ADA  
039161



END

DATE

FILMED

6-77

ADA039161

1

DDC  
RECEIVED  
MAY 10 1977  
C

AN INVESTIGATION OF LASER-TARGET  
INTERACTION SIGNALS

THESIS

GEP/PH/75-14      RICHARD D. ARLEN, JR.  
CAPTAIN      USAF

Approved for public release; distribution unlimited.

(See form 1473)

**AN INVESTIGATION OF LASER-TARGET  
INTERACTION SIGNALS**

**THESIS**

**Presented to the Faculty of the School of Engineering  
of the Air Force Institute of Technology  
Air University  
in Partial Fulfillment of the  
Requirements for the Degree of  
Master of Science**

**by**

**Richard D. Arlen, Jr., B.S.  
Captain USAF  
Graduate Engineering Physics  
December 1975**

**Approved for public release; distribution unlimited.**

## Preface

This study was sponsored by the Air Force Flight Dynamics Laboratory. It is part of a series of investigations designed to develop the theory and instrumentation necessary to predict jet engine failures. The proposed system would require both a particle detector and an excess charge detector in the jet exhaust. An engine component which is located near the exhaust would release a large number of particles when it begins to fail. These particles would be detected by the particle detector. Internal components that fail further from the exhaust produce few, if any, particles in the exhaust. This condition would be detected by the excess charge detector.

I would like to express my sincere appreciation to Dr. S. R. Lyon and Mr. J. Schell of the Air Force Materials Laboratory (AFML) for the assistance they provided. Mr. Schell supplied the majority of the targets and Dr. Lyon provided expert knowledge on the metallurgical aspects of this study. Also, I would like to thank Major R. P. Couch, my thesis advisor, and Captain P. E. Nielsen for the guidance and encouragement they each provided. I also extend my appreciation to the Air Force for allowing me the opportunity to continue my education.

Finally, I would like to thank my wife and children

for cheerfully enduring their many hours of loneliness  
brought about by my AFIT tour.

Richard D. Arlen, Jr.

ADMISSION for	
NTIS	White Section <input checked="checked" type="checkbox"/>
DEC	Buff Section <input type="checkbox"/>
UNANNOUNCED	
JUSTIFICATION	
BY	
DISTRIBUTION/AVAILABILITY CODES	
Dist.	AVAIL. OR SPECIAL
A	

Contents

	Page
Preface.....	11
List of Figures.....	vi
List of Tables.....	viii
Abstract.....	ix
I. Introduction.....	1
Purpose.....	1
Background.....	2
Approach.....	3
Scope.....	3
Organization.....	4
II. Equipment and Materials.....	5
Equipment.....	5
Air Supply.....	6
Stagnation Chamber.....	6
Stress Chamber.....	7
Particle Separator.....	8
Faraday Cage.....	10
Laser.....	10
Photo Detector.....	12
Integrator.....	12
Oscilloscopes.....	13
Materials.....	13
III. Interpretation of Signals.....	16
Laser-Target Signals.....	16
Region I.....	17
Region II.....	17
Region III.....	18
Region IV.....	19
Particle Separator Signals.....	19
IV. Experiments.....	21
Introduction.....	21
Laser-Target Signals.....	21
Region I.....	21
Region II.....	24
Region III.....	27

	Page
Region IV.....	32
Additional Experiments.....	35
Simulated Jet Engine.....	40
Pipe Signal.....	40
Particle Separator.....	41
Faraday Cage.....	41
V. Results and Recommendations.....	44
Results.....	44
Laser-Target.....	44
Pockets.....	47
Recommendations.....	48
Bibliography.....	49
Appendix A.....	51
Vita.....	71

## List of Figures

<u>Figure</u>		<u>Page</u>
1	Schematic of the simulated jet engine .....	5
2	Stress Chamber (actual size).....	8
3	Exposed View of Particle Separator.....	9
4	Photo Detector.....	12
5	Integrator.....	13
6	Target signal broken in four regions.....	16
7	Target signal for thick oxide Ni target.....	17
8	Plume-target interaction.....	18
9	Illustrative target damage.....	18
10	Particle separator.....	20
11	Illustrative Particle Separator Signals.....	20
12	Illustrative effect of oxide on target signals.	22
13	Effect of oxide on Ni and Fe target signals....	23
14	Target mounting techniques.....	24
15	Target signals for Fe, Ni, and Ge.....	25
16	Target signal for cold-rolled steel.....	26
17	Cold-rolled steel mounted at an angle.....	26
18	Target signals for clean cold-rolled steel.....	27
19	Target signal and associated damage for thin oxide Fe.....	28
20	Target signal and associated damage for thin oxide Fe.....	29
21	Target signal and associated damage for thin oxide Ni.....	30
22	Target signal and associated damage for thin	

<u>Figure</u>		<u>Page</u>
	oxide Ni.....	31
23	Target signals for the cathode material, clean cold-rolled steel, and thin oxide Fe.....	33
24	Clean cold-rolled steel signals.....	33
25	Oxide layer for cold-rolled steel.....	34
26	Illustration of Fig. 27.....	35
27	Clean Cb target signal. 9KV/30"(11Sep).....	35
28	Illustrative target signals for cold-rolled steel.....	36
29	Illustrative target signals for cold-rolled steel (6"Hg).....	37
30	Biased and un-biased target signal for Clean Ni	38
31	Pipe signal for cold-rolled steel.....	41
32	Box and blade signals for Ni and Ti.....	42
33	Signals for thick oxide Ti.....	42
34	Generation of positive pocket by oxidation.....	43

### List of Tables

<u>Table</u>		<u>Page</u>
I	Pressure (inches Hg) vs Air Speed (ft/msec)....	7
II	Laser Energy vs Supply Voltage.....	11
III	Time and Temperature Used to Prepare Oxides....	14

Abstract

Micro distresses were created in a simulated jet engine using a pulsed ruby laser, and the electrical signals were studied at various points in the simulator. Average power levels at the target ranged from  $4.0 \times 10^5$  to  $4.77 \times 10^6$  watts per square centimeter. Target materials investigated were cold-rolled steel, Ti 64, Mn, Co, a cathode material, and high purity Fe, Ni, Ti, and Cb. It was found that the target signals have a reproducible pattern. The most general pattern observed could be separated into four regions and had the general appearance of two cycles of a sine wave. With the possible exception of the cathode material, the interpretation applied to each region was independent of the target material used. The interpretation applied to each region was: Region I - laser induced thermionic emission, Region II - plume-target interaction, Region III - thermionic emission from the hot flushed material, and Region IV - oxide tail formation due to the plume-target interaction. A leading portion of Region I correlated with the thickness of the oxide layer on the target, and in the absence of airflow, Region II correlated with the depth of the hold. It was found that the blow-off from the cathode material and Ni had negative particles and produced positive pockets upon passage through the simulator - the simulator basically removed charged particles from the air stream. All other materials produced positive particles and negative pockets. It was also found that oxidation produced

positive pockets. These experiments substantiate the Positive Pocket Theory proposed by Couch and suggest expanding it to include negative pockets.

# AN INVESTIGATION OF LASER-TARGET INTERACTION SIGNALS

## I. Introduction

### Purpose

The initial purpose of this study was to verify the Positive Pocket Theory presented by Couch (Ref 1:6). This theory assumes pockets of excess ion charge are created in a particle plasma mixture when the charged metal particles are mechanically removed - this removal leaves a compensating ion charge in the gas stream with a polarity opposite to that of the particles removed. The verification involved irradiating a target with a pulsed ruby laser and electrically monitoring the flow of the blow-off material through a simulated jet engine. Initially, the maximum laser output was about 20 joules/pulse. These shots produced from 20 to 30 nanocoloumbs of excess negative charge and suggests expanding the initial theory to include negative pockets. During the investigation it became necessary to reduce the laser output to a maximum of about 10 joules/pulse to correct a laser pre-firing problem. At this lower output, it was observed that the waveform of the electrical signal from the target had altered - it now had the general appearance of two cycles of a sine wave. At this time the purpose of this study was changed - the new purpose was to attempt to understand the meaning of the sinusodial nature of the target signal.

## Background

In November 1970, Captain R. Vopalensky was collecting data in support of his master's thesis. This thesis (Ref 2) involved the use of an electrostatic probe in the exhaust of a J-57 jet engine. While collecting data, relatively large transient signals began to be detected by the probe. At first, the transient spikes were attributed to a malfunction in the probe electronics. However, the electronics proved to be operating correctly; therefore, the spikes continued to be monitored. It was observed that both the frequency and amplitude of the spikes were increasing; however, the source of the spikes was unknown. The engine failed due to a fatigue fracture at the base of a second stage turbine blade on the second day of monitoring.

A particle-probe interaction theory (Ref 3, 4) was proposed to explain the presence of spikes in the J-57 engine. This theory made the following two assumptions: (1) when the engine began to fail, charged metal particles were ejected into the air stream by the fatigued component, and (2) these charged particles were responsible for the observed transient spikes. This theory was rejected because the calculated waveform could not account for the spikes. However, the calculated waveform did agree with some signals that were observed in jet engines.

The next theory (Ref 5) assumed the probe built up a positive ion sheath which was discharged by a particle. This theory was rejected because metal particle ingestion

did not produce spikes and a theoretical analysis (Ref 6) proved the sheath could not exist.

The most recent theory (Ref 1:6) is that spikes, which have been identified as Trichel pulses (Ref 7: 33), are produced by positive pockets. A Trichel pulse is an intermittent negative corona discharge. This theory makes the following assumptions: (1) when an engine begins to fail, metal particles and a plasma are simultaneously liberated into the air stream, (2) the plasma charges the particles negatively, (3) the charged metal particles become lost in the engine, and (4) the resultant positive pocket is of sufficient strength to produce Trichel pulses.

#### Approach

The approach used in this study was to create microdistresses in a simulated jet engine using a pulsed ruby laser and then look for correlations among the electrical signals which were monitored at various points in the simulator. If correlations were found, then their generality would be checked using different target materials.

#### Scope

This study generated approximately 1900 photographs or equivalently 950 data points. Each data point is composed of two photographs and each photograph has two signals recorded. The maximum average power initially used was  $1.3 \times 10^7$  watts per square centimeter. However, when the pre-firing problem occurred, this value was lowered to  $4.8 \times 10^6$ . The materials studied in detail were cold-rolled

steel, Ti 64, and high purity Fe, Ni, Ti, Cb, and Ge. The materials cursorily examined were Mn, Co, and a cathode material which had Ni particles embedded in it - the particles were approximately ten microns in diameter.

### Organization

This thesis is divided into five sections. The introduction gives the reader some background into the previous studies which are pertinent to this thesis. Furthermore, the approach used and the scope of the study are also given. The second section presents the equipment and materials used in the investigation. A schematic of the equipment is given in Fig. 1. It is important that the reader read and understand the notation developed in the materials section. The notation refers to how the materials were prepared. The third section interprets the electrical signals encountered in this study - the signals are categorized into laser-target and particle separator. The fourth section presents experiments used to verify the interpretation of the laser-target interaction signal and experiments pertaining to the simulator. The last section discusses the results of this thesis and then gives recommendations for further investigations.

## II. Equipment and Materials

### Equipment

Figure 1 illustrates the equipment used in this study.

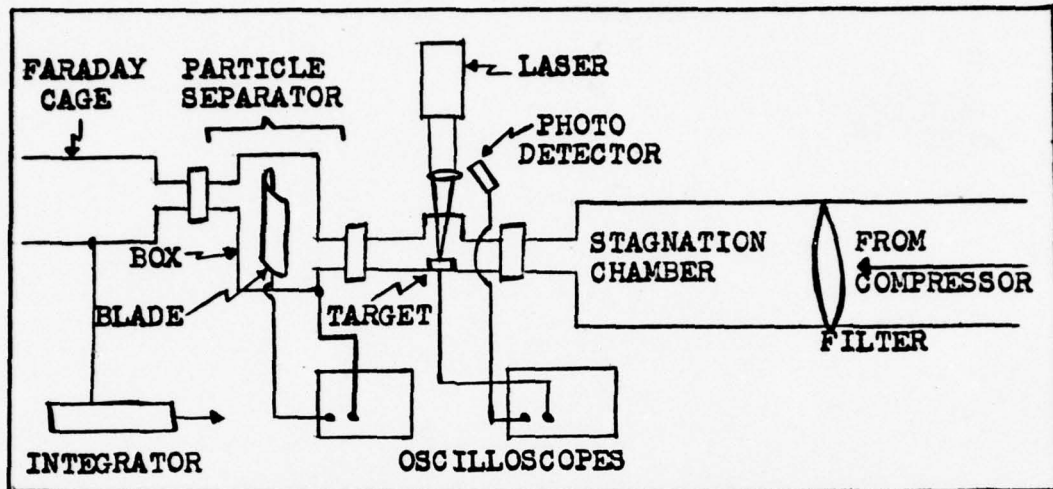


Fig. 1. Schematic of the simulated jet engine.

The purpose of the laser was to simultaneously liberate metal particles and a plasma from the target - this fulfilled the first requirement of the Positive Pocket Theory. This blow-off material was then swept downstream to the particle separator. The blade removed metal particles from the blow-off and simulated charged metal particles becoming lost in the engine - the third requirement of the theory. The resulting pocket (blow-off material minus particles which hit the blade or were lost in the box) then flowed through the Faraday Cage, which allowed calculation of the total charge in the pocket. It was necessary to relinquish one channel of the oscilloscope when the Faraday Cage was monitored. Either the box, blade, or box plus blade was

monitored in conjunction with the Faraday Cage. The particular signal depended on what was being studied at the time.

Air Supply. Pressurized air was generated by a Worthington #YB-2 compressor which was equipped with a \* Electrodryer #B2 electric air dryer. The compressor was capable of delivering 100PSI at a flow of 500 cubic feet per minute to the stagnation chamber. Prior to entering the stagnation chamber, the air was filtered with a porous filter paper (0.90 micron pore size).

Stagnation Chamber. Pressure in the stagnation chamber was monitored with a mercury manometer and corresponded to an air speed in the simulator. To obtain an estimate of the air speed in the simulator, a pitot tube was inserted into the air stream at the exit of the stress chamber and the stagnation pressure in the air flow was recorded. It was assumed that the free stream pressure remained equal to the atmospheric pressure (29.1 inches of Hg). The air speed was determined as follows: (1) divide the atmospheric pressure by the sum of the pressure measured by the pitot tube and the atmospheric pressure, (2) find the correspond-

---

\*  
Water vapor was always present in the air supply and would sometimes condense on the window of the stress chamber. The air supply became contaminated with oil near completion of this study. Its effect on the polarity of the pocket is discussed by Mitchell (Ref 8).

ing value of the Mach number M (Ref 9:614,615), and (3) multiply the value of M by 1128.53 ft/sec (Ref 9:75,80,81). For example, a measured pressure of 10.0 inches of Hg yielded a ratio of 0.8291. This value corresponded to an M value of 0.52; therefore, the velocity was 586.84 ft/sec. When the pitot pressure was above 26 inches, a velocity greater than Mach 1.0 was predicted although Mach 1 velocities were not achieved in this study. The error in the calculation was due to the incorrect assumption that the free stream pressure was equal to the atmospheric pressure. Table 1 summarizes the air speed calculations.

Table I

Pressure (inches Hg) vs Air Speed (ft/msec)

Stagnation Pressure	5	10	15	20	30	40	50
Pitot Pressure	3.5	6	9	12	17.5	20	26
Mach #	0.41	0.52	0.63	0.72	0.85	0.90	1.0
Air Speed	0.46	0.59	0.71	0.81	0.95	1.0	1.13

Stress Chamber. The stress chamber (Fig. 2) coupled the laser-target blow-off material to the air flow. In operation, the target holder was situated at point A (Fig. 2). A 2/56 brass screw and nut held the target to the holder. The target holder was then attached to the holder cap with a 6/32 brass nut. Six 6/32 brass screws were used to secure the holder to the body. The window was fused silica and quartz and was 1 x 1/8 inch. It was held in place by

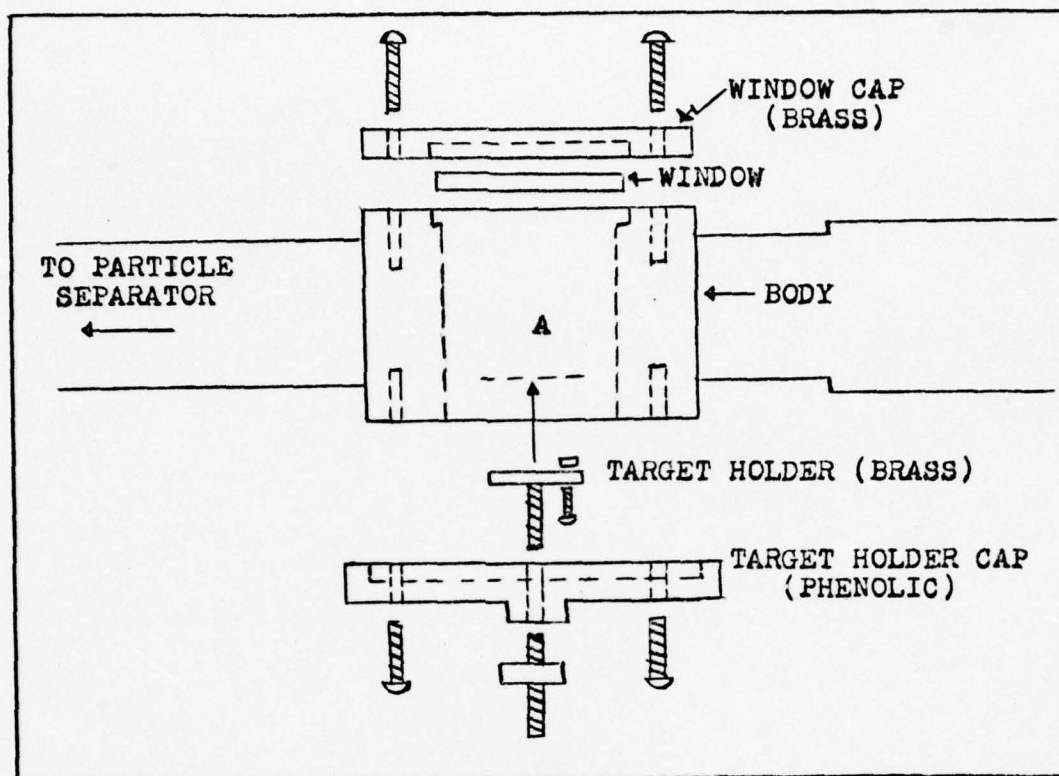


Fig. 2. Stress Chamber (actual size).

the window cap which was secured to the body by six 6/32 brass screws. Copper tubing (3/4 inch) was used to channel the air flow thru the body. Finally, the tubing on the input section of the body had a 3/4 inch copper coupler soldered to it.

Particle Separator. The box and the blade (Fig. 3) constituted the particle separator. The box had the following dimensions: 3.5 inches wide, 4.5 inches long, and 4.0 inches high. It was constructed from 1/8 inch brass and had a 3/8 inch thick brass flange soldered to the top and bottom. The top was made of 1/8 inch aluminum and the bottom from 3/8 inch laminated phenolic.

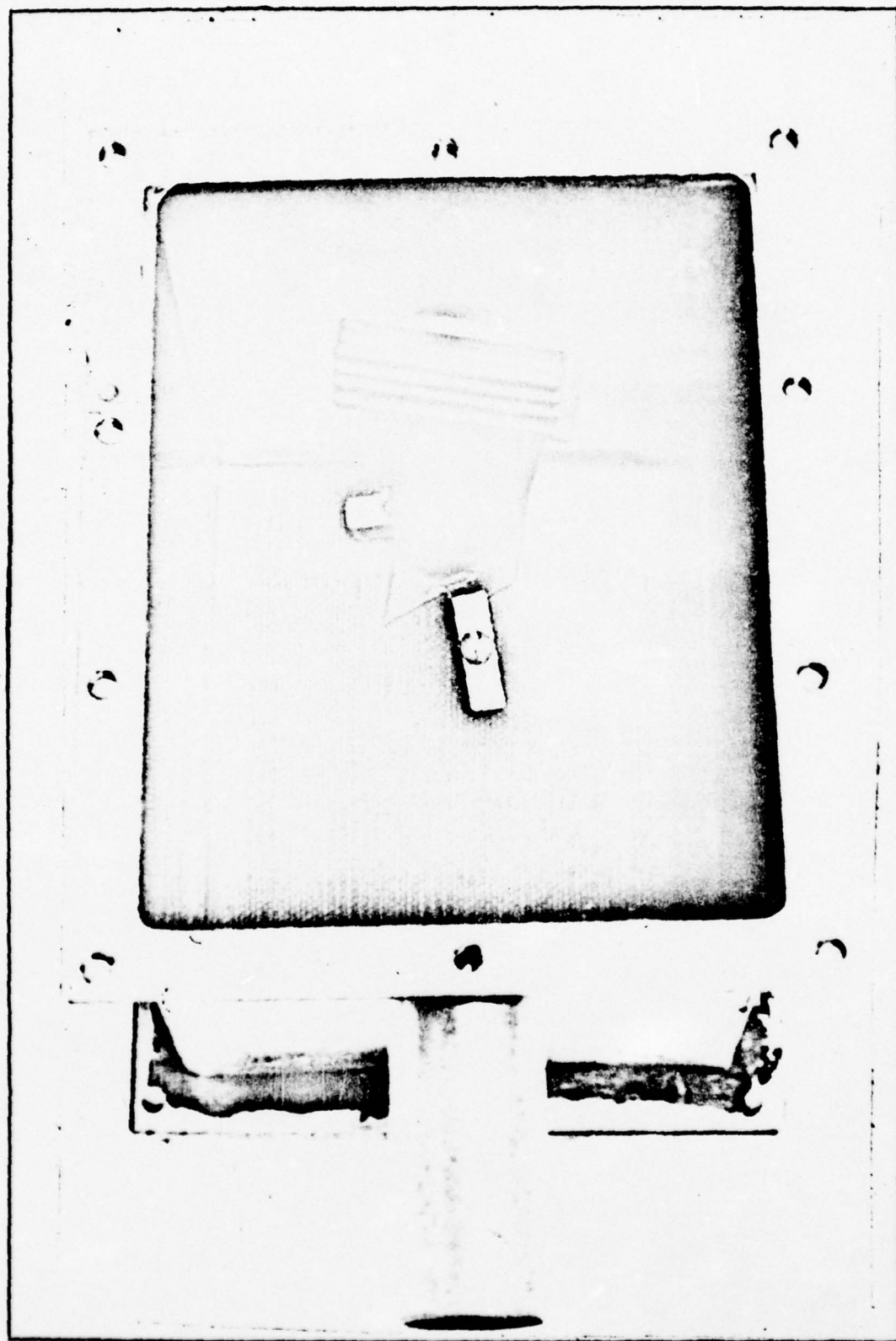


Fig. 3 Exposed View of Particle Separator

The blade used was a turbine blade from a jet engine. It was attached to the phenolic by two 1.0 inch aluminum bars. The bar on the concave side of the blade was attached with a screw. The other bar was bolted to the phenolic. This bolt served as the electrical pickup point for the blade signal.

In operation, the bottom (phenolic) of the box was wrapped with aluminum foil on the outside so that the aluminum was in direct contact with the metal sides of the box. The box was then enclosed in a cardboard box which was wrapped with grounded aluminum foil. This was done to shield the particle separator from any stray electrical pickup.

Faraday Cage. The purpose of the Faraday Cage was to allow calculation of the net charge of the pocket. It was constructed of zinc coated sheet metal, was 69 inches long, and had a 7 inch diameter. Copper tubing (3/4 inch) was soldered to the end which faced the particle separator. In operation, the Faraday Cage was first wrapped with paper and then with aluminum foil. The foil was grounded to eliminate stray pickup.

Laser. The laser used was a water cooled pulsed ruby laser (Korad K-2000). The maximum pulse width was approximately 0.8 milliseconds. Each pulse contained spikes approximately one microsecond wide with two microseconds between spikes. The laser delivered a maximum average energy of 20.8 joules per pulse when the investigation

began. This value was lowered to 10.0 to correct a pre-firing problem. The energy in the pulse vs the supply voltage is given in Table II.

Table II

Laser Energy vs Supply Voltage

<u>Supply Voltage (KV)</u>	<u>Energy (J)</u>	<u>Average Energy (J)</u>
8.6	0.06, 0.096, 0.155 0.14, 0.0175, 0.08 0.075	0.11
9.0	1.5, 1.8, 1.8, 1.7	1.70
9.5	5.1, 5.0, 5.1, 4.9 5.3, 4.65, 4.9	4.99
10.0	9.25, 10.5, 10.25 9.75, 10.25	10.0

The average power was calculated as follows: (1) determine the number of spikes in the pulse by dividing the pulse width by the average time between spikes (3 us), (2) determine the effective time of the laser by multiplying the number of spikes in the pulse by 1 us - the duration of one spike, and finally, (3) divide the laser energy by the effective time of the laser. For example, the 10.0 joule pulse had 267 spikes (.8 ms/3 us). The effective time of the laser was 267 us (267 x 1 us). This produced a power of  $3.75 \times 10^4$  watts (10 J/267 us). This energy was focused by a 101.6 mm lens and always produced a hole whose diameter was approximately 1.0 mm. Therefore the area of the 1.0 mm hole was taken to be the standard area over which the laser

energy was distributed. For example, the standard area yielded a power density of  $4.77 \times 10^6$  watts per square centimeter for the 10.0 joule pulse.

Photo Detector. The photo detector (Fig. 4) served

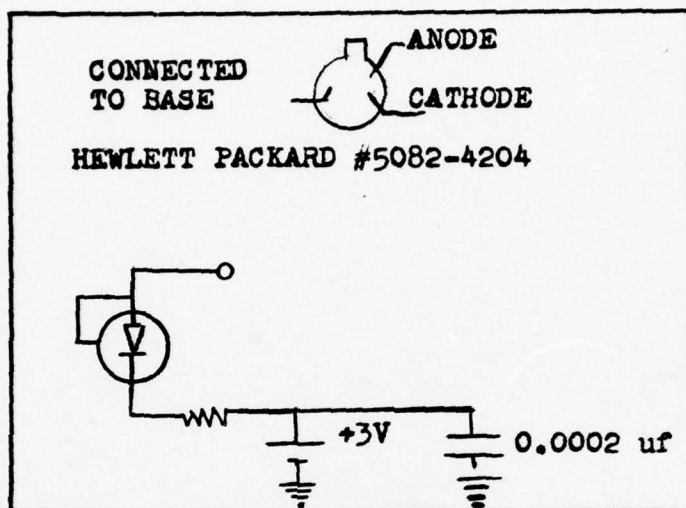


Fig. 4. Photo Detector.

two purposes. First it allowed the laser signal to be recorded in conjunction with the target signal. It was also used to trigger both oscilloscopes.

Integrator. The purpose of the integrator (Fig. 5) was to electronically sum the total charge in the Faraday Cage. The integrator produced a 10 mv inverted signal for each nanocoloumb of charge that flowed through the Faraday Cage. For example, a negative 10 mv signal from the integrator corresponded to a positive pocket having a total charge of 1.0 nanocoloumb. The output voltage of the integrator was fed directly to the oscilloscope.

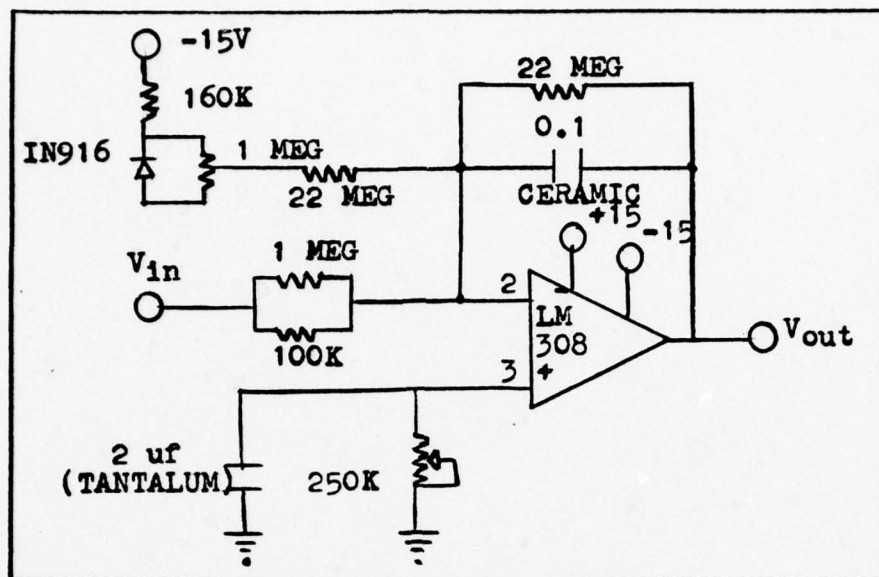


Fig. 5. Integrator

Oscilloscopes. Two Tektronix (#7904) oscilloscopes were used. Each had two amplifiers (#7A16A). The time base unit on one oscilloscope was #7B70 while the other was #7B92. The input impedance used was one megohm.

#### Materials

The materials used in this study were cold-rolled steel, Mn, Co, a cathode material, Tl 64, and the following high purity materials: Fe, Ni, Ti, Cb, and Ge. The surfaces of the Fe, Ni, Ti, and Cb were prepared by the Air Force Materials Laboratory; the cold-rolled steel was prepared by the author, and the rest were used on an as received basis.

The surfaces of the Fe, Ni, Ti, and Cb were prepared in 2 x 2 inch squares and polished using the following

successive grit sizes: 180, 240, 320, 400, and 600. The final average groove size (peak to valley) was approximately 32 to 40 microinches. The targets were then washed. The wash consisted of the following steps: (1) wash with soap and water, (2) wash with methanol, (3) blow dry with compressed air, (4) wash with ethanol, and (5) swab with ethanol using a sterile swab. The term "clean," when applied to one of these metals, means that the target was prepared in the above manner. The thickness of the Fe, Ni, Ti, and Cb were respectively 80.0, 24.5, 38.5, and 30.0 mils.

Another batch was prepared as above for the purpose of investigating the role of oxides. A thin oxide layer was grown on half the batch and a thicker oxide layer was grown on the other half. Hence the term "thin" and "thick" are used to refer to the oxide thickness. The time and temperature used to prepare the oxides for each metal is given in Table III.

Table III

Time and Temperature Used to Prepare Oxides

METAL	OXIDE THICKNESS	
	THIN	THICK
Fe	3 min @ 470 C	4 hrs @ 470 C
Ti	4 min @ 750 C	4.5 hrs @ 750 C
Cb	5 min @ 400 C	45 min @ 400 C
Ni	15 min @ 400 C	4.5 hrs @ 400 C then 16 hrs @ 825 C

One of the clean Ni surfaces was polished with Magomet (MgO) and then washed as described before. The term "polished," when applied to Ni, means that the target had been prepared in the above manner.

Some of the cold-rolled steel targets were polished by the author using the following grit sizes: 180, 240, 320, 400, and 600. These targets were then cleaned with ethanol and are referred to as clean cold-rolled steel.

The cathode material was supplied by the Air Force Avionics Laboratory and was 39.37 mils thick. A mixture of Ba, Sr, and Ni carbonates on a Ni base comprised the cathode material.

All targets were cleaned with ethanol prior to each experiment. Therefore, if only the name of the material is mentioned, it was only cleaned with ethanol prior to the experiment.

### III Interpretation of Signals

#### Laser-Target Signals

A discussion of the electrical signals from targets situated in an air stream which are irradiated with a pulsed ruby laser is presented in this section. With the possible exception of the cathode material, a strong correlation was found between the target signal and the observed target damage. The target material used to establish the correlation was cold-rolled steel. However, the correlation has been checked using Ti 64 and high purity Fe, Ni, Ti, and Ge. The experiments verifying these interpretations are presented in section IV.

Figure 6 (not to scale) is an illustrative example of the signals observed when cold-rolled steel was irradiated.

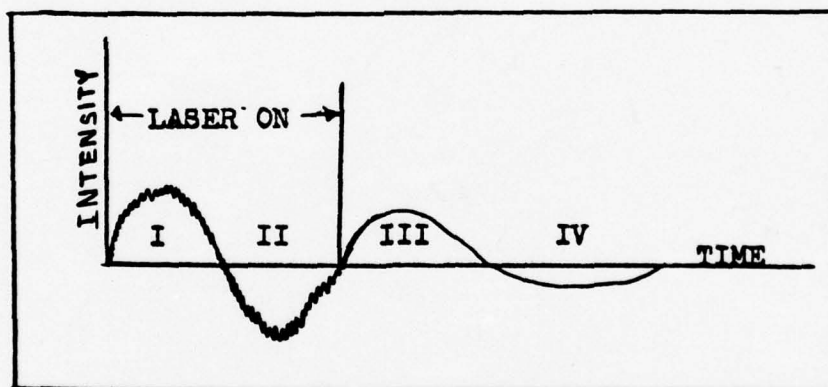


Fig. 6. Target signal broken in four regions. The target signal illustrated in Fig. 6. consists of four regions, whose interpretation is as follows:

- (1) Region I - Laser induced thermionic emission.
- (2) Region II - Plume-target interaction.

(3) Region III - Thermionic emission from the hot flushed material.

(4) Region IV - Oxide tail formation due to the plume-target interaction.

Region I. Region I is interpreted as being due to thermionic emission and has the general appearance shown in Fig. 7. The lower trace is the laser signal and the upper trace is the target signal for nickle which has an oxide thickness of approximately 0.33 mil. The step appearance, which follows the surface temperature, is characteristic of thermionic emission; the spikes are not.

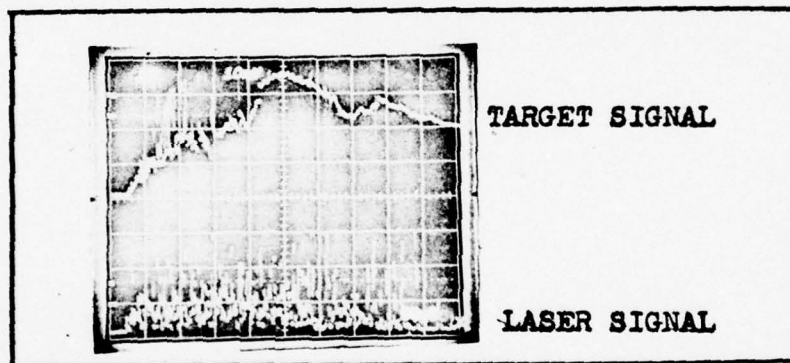


Fig. 7. Target signal for thick oxide Ni target.

Lichtman and Ready (Ref 10) state that the spikes are also due to thermionic emission. Giori et al (Ref 11) show that although there is a time correlation between the target spike and the associated laser spike, there appears to be no correlation between their intensities.

Region II. Region II is interpreted as being due to the plume interacting with the hole and downstream surface of the target as illustrated in Fig. 8. The plume is a

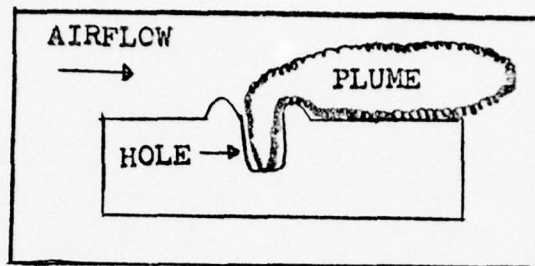


Fig. 8. Plume-target interaction.

plasma and contains electrons and ions. Seshadri (Ref 12:77) shows that for all practical purposes, the average thermal speed of the electrons is greater than that of the positive ions. Therefore, more electrons than positive ions can migrate to the surface of the target - the target signal can go negative. If the plume-surface interaction is minimized (no airflow), the target signal will go more negative as the depth of the hole increases because the plume-hole coupling time increases.

Region III. Region III is interpreted as being due to thermionic emission from the hot flushed material (Fig. 9.).

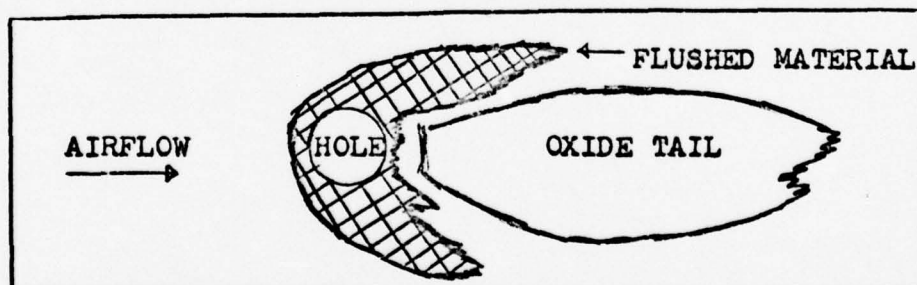


Fig. 9. Illustrative target damage.

The flushed material (Ref 13:118) consists of liquid metal which was first washed to the surface as the plume flowed out of the hole, and then washed across the surface by the

airflow. The metal is hot and will thermionically emit electrons to the air stream - this drives the target signal positive.

Region IV. Region IV is interpreted as being due to the formation of an oxide tail (Fig. 9). The downstream surface is heated when the plume is swept across it and this leads to the oxide formation. The reason the signal goes negative is that negatively charged oxygen migrates to the surface and forms an oxide.

Per Kofstad (Ref 14:11) states that "A detailed understanding of the oxidation behavior of a metal requires knowledge of reaction rates and kinetics, the temperature and oxygen pressure dependence of the reaction, and the composition, structure, and growth mechanism of the reaction products." The data gathered in this study did not permit the above analysis. However, the interested reader is referred to Per Kofstad for a discussion of the above parameters. This book gives an excellent discussion of the oxidation rates of Ti (169-178) and Cb (209-221).

#### Particle Separator Signals

The particle separator (Fig. 10) removed metal particles from the blow-off material. The blow-off material had a net negative charge and was first sensed by the box and then by the blade. When positive metal particles separated from the blow-off material and struck the blade, the blade signal went positive. At the same time, the box signal went negative because the box sensed an increased negative charge

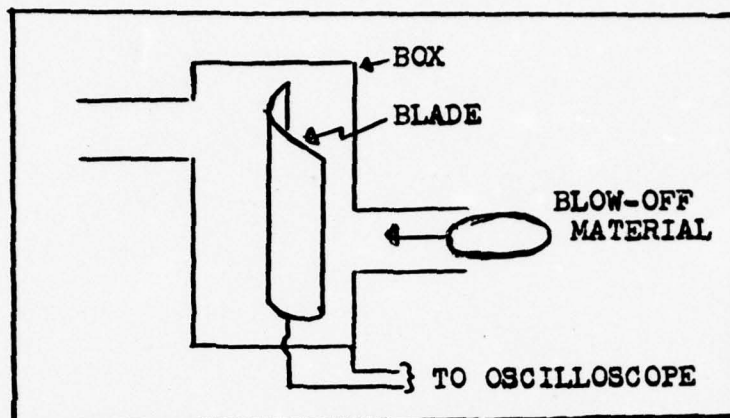


Fig. 10. Particle separator.

when the blade subtracted the positive metal particles from the blow-off material. A negative pocket leaving the box is indicated by a positive box signal. These signals are illustrated in Fig. 11.

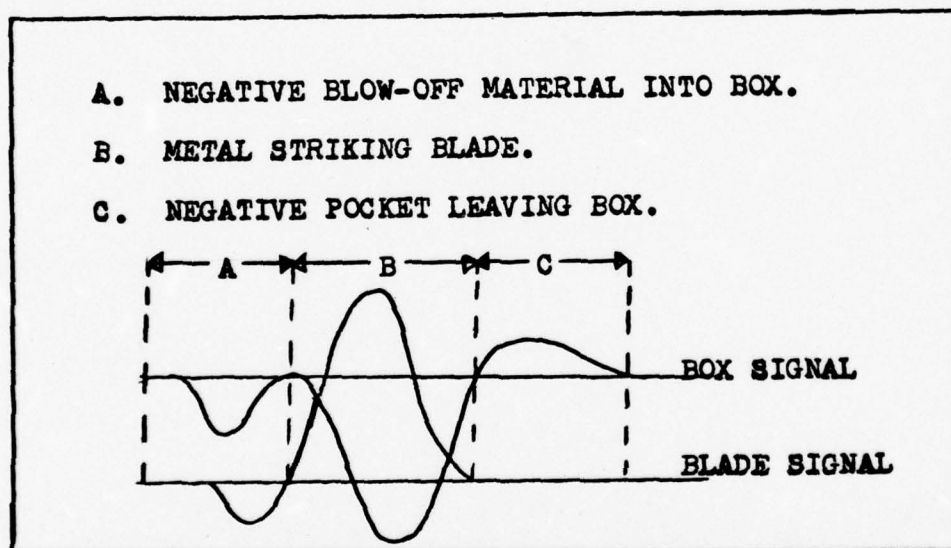


Fig. 11. Illustrative Particle Separator Signals.

## IV. Experiments

### Introduction

The purpose of this chapter is to show the results of experiments pertaining to the laser-target interaction and the simulated jet engine. Only a limited number of pictures appear in this chapter; however, Appendix A contains a sampling of signals from each material studied. During the course of this study, the photo detector had been accidentally moved on several occasions. Although an attempt was always made to return the detector to its original position, there was no way to verify that the repositioning was accurate. To alleviate this situation, the date will always be given. For example, 9KV/30" (15 Aug.) will mean the laser supply voltage was 9,000 volts, the pressure in the stagnation chamber was 30 inches, and the data was collected on August 15. The reader is warned against comparing laser intensities on different dates.

### Laser-Target Signals

As shown in the previous chapter, the most general target signal observed in this study could be separated into four regions. With the possible exception of the cathode material, the interpretation applied to each region was independent of the target material. For this reason, different materials were used in verifying the four regions. Following the verification, supplemental data pertaining to the laser-target interaction is presented.

Region I. Region I is due to thermionic emission and

will produce a positive target signal. The technique used to verify Region I was based on the fact that thermionic emission from a surface is sensitive to surface conditions (Ref 15:140); in particular, oxide thickness. Therefore, the target signal should reflect any oxide thickness which is present on the surface - the target signal should have a sudden change in slope when the laser begins interacting with the metal base. Figure 12 illustrates the portion of the signal due to the oxide and Fig. 13 shows the effect of oxide on Ni and Fe target signals. Figure 13(d) reflects the fact that the thick oxide Ni was actually composed of two separate and distinct layers. Since the target signal is sensitive to the oxide layer, it is concluded that Region I is due to thermionic emission.

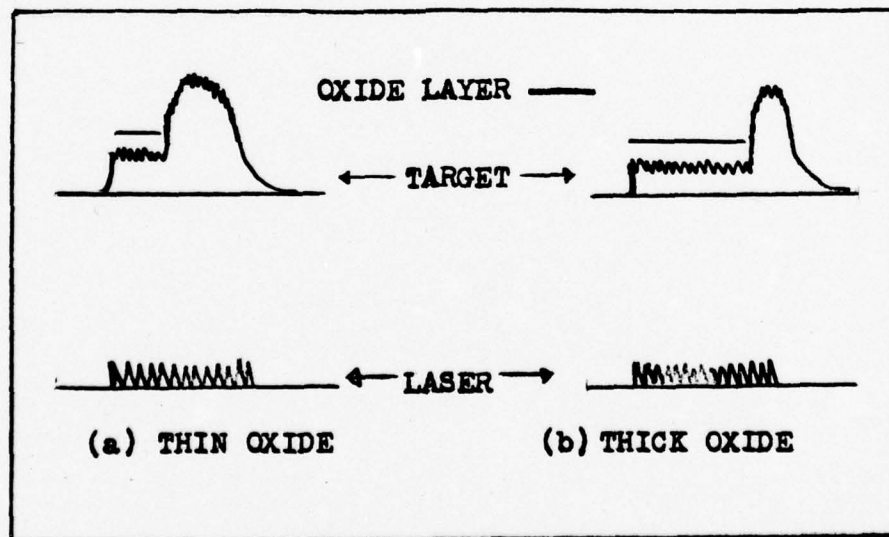
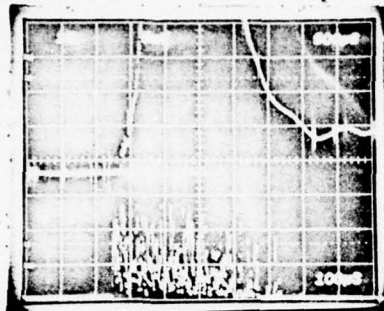
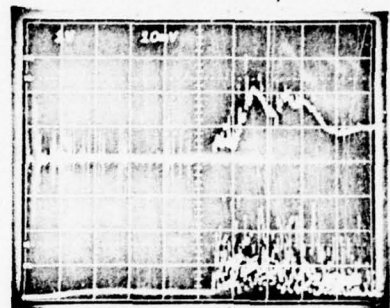


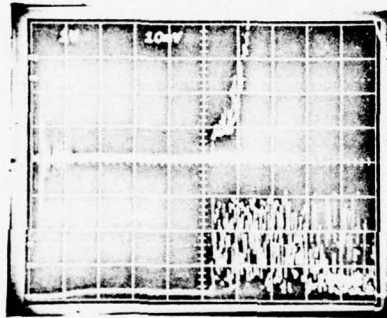
Fig. 12. Illustrative effect of oxide on target signals.



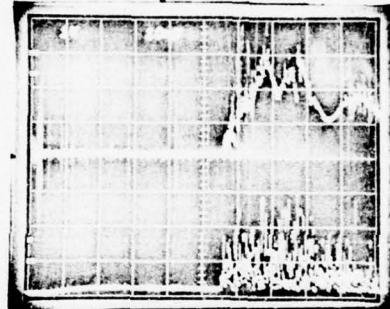
(a) Polished Ni  
9.4KV/40" (19Sep)



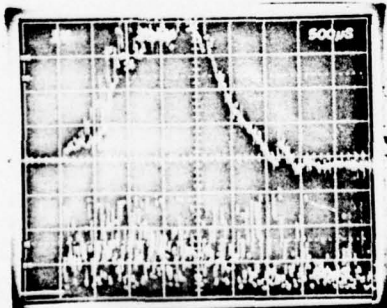
(b) Thin oxide Ni  
9.3KV/40" (18Sep)



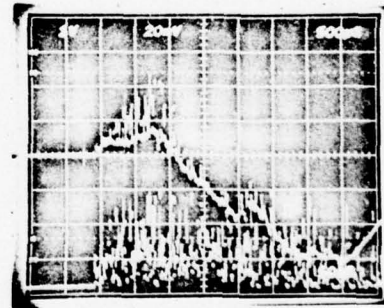
(c) Thin oxide Ni  
9.3KV/40" (18Sep)



(d) Thick oxide Ni  
9.4KV/30" (18Sep)



(e) Thick oxide Fe  
9.45KV/40" (18Sep)



(f) Thick oxide Fe  
9.45Kv/32" (18Sep)

Fig. 13. Effect of oxide on Ni and Fe target signals.

Region II. Region II is due to the plume interacting with the target and produces a negative target signal because the plume drives electrons to the target. The verification of this region is divided into two categories - plume-hole and plume-surface. The approach used in the verification was to make the effects of the category of interest greater than the effects of the one which was not of interest.

The plume-hole interaction was studied with no airflow. This decreased the plume-surface interaction. A paper shield was constructed to reduce any effects which the plume might have on the target holder. The techniques used to mount the targets are illustrated in Fig. 14. The target materials

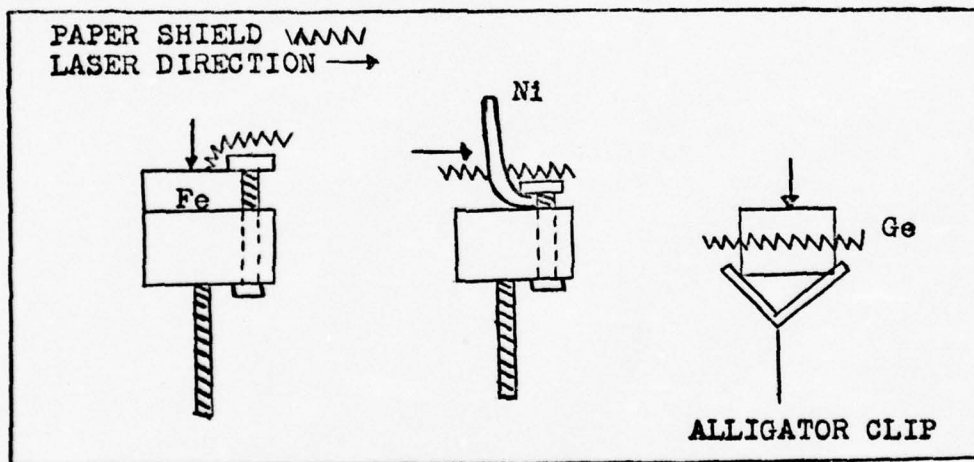
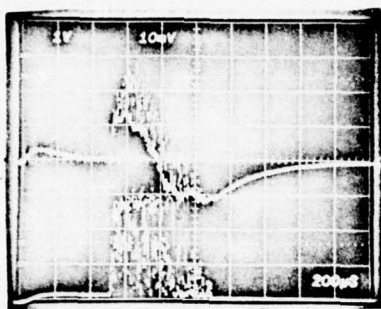


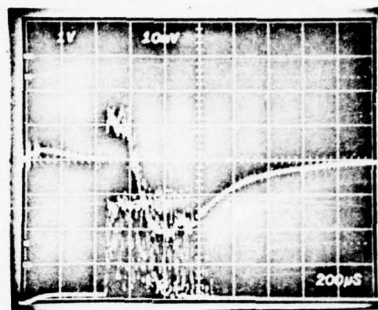
Fig. 14. Target mounting techniques.

used were clean Fe, thin oxide Ni, and Ge. The signals are given in Fig. 15. A visual observation of the hole depth confirmed that the deeper the hole, the more negative the signal went.

CLEAN Fe.....9.5KV/0"(60Oct)

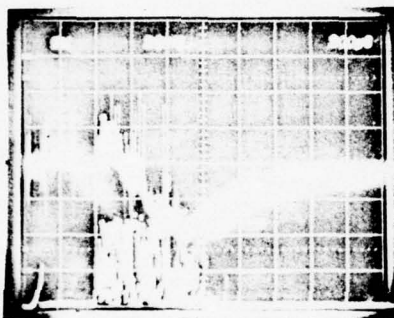


(a)

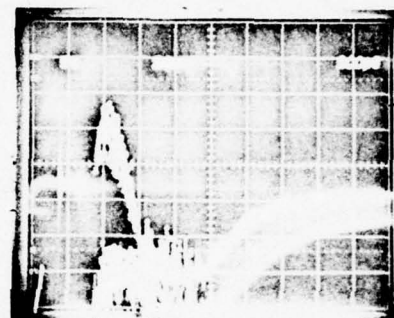


(b)

THIN OXIDE N1.....10KV/0"(70Oct)

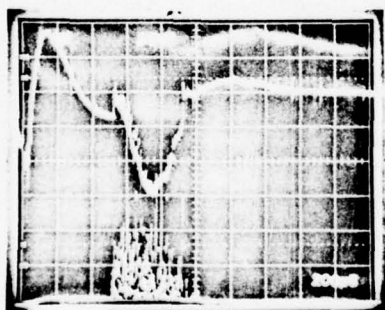


(c)

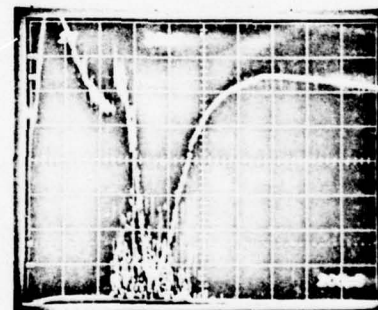


(d) Hole punched thru metal\*

Ge.....9.5KV/0"(13Sep)



(e)



(f)

Fig. 15. Target signals for Fe, N1, and Ge.

\*The point of focus was inside the target. No hole was blown thru the target when the point of focus was on the surface.

The plume-surface interaction was studied with airflow. The effect of the plume was minimized by irradiating the target about one spot diameter from the downstream edge (Fig. 16(b)). Its effect was maximized by tilting the target (Fig. 18). Figure 17 illustrates the method used to tilt the target. These examples clearly show that the plume-surface interaction does drive the target signal negative.

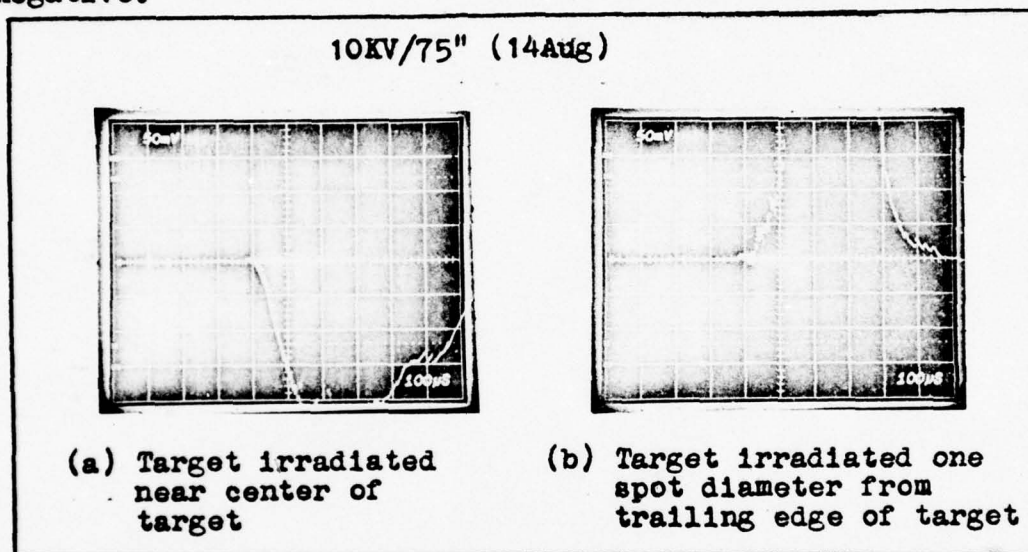


Fig. 16. Target signal for cold-rolled steel.

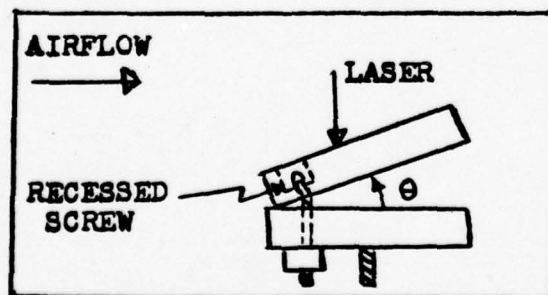


Fig. 17. Cold-rolled steel target mounted at an angle.

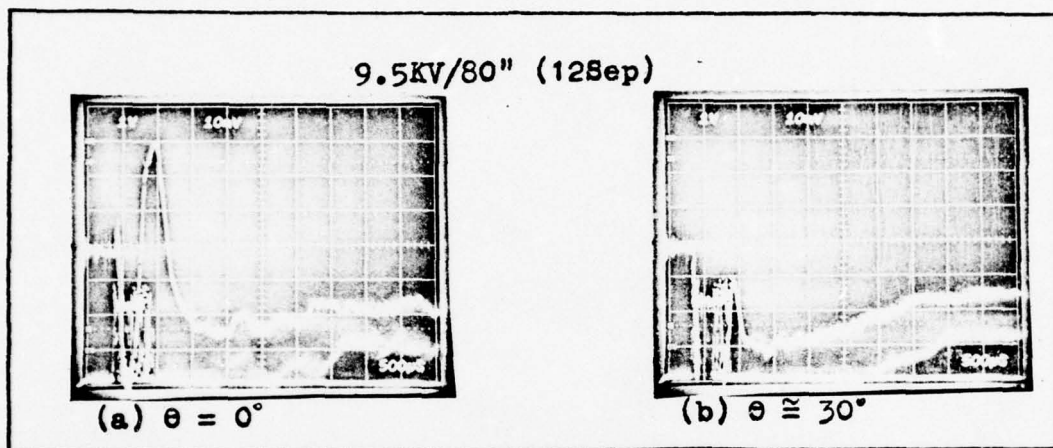
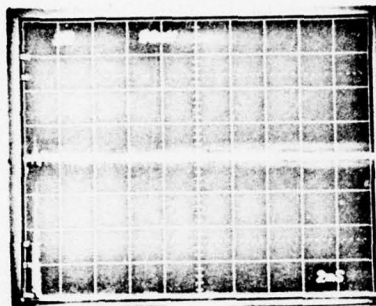


Fig. 18. Target signals for clean cold-rolled steel.

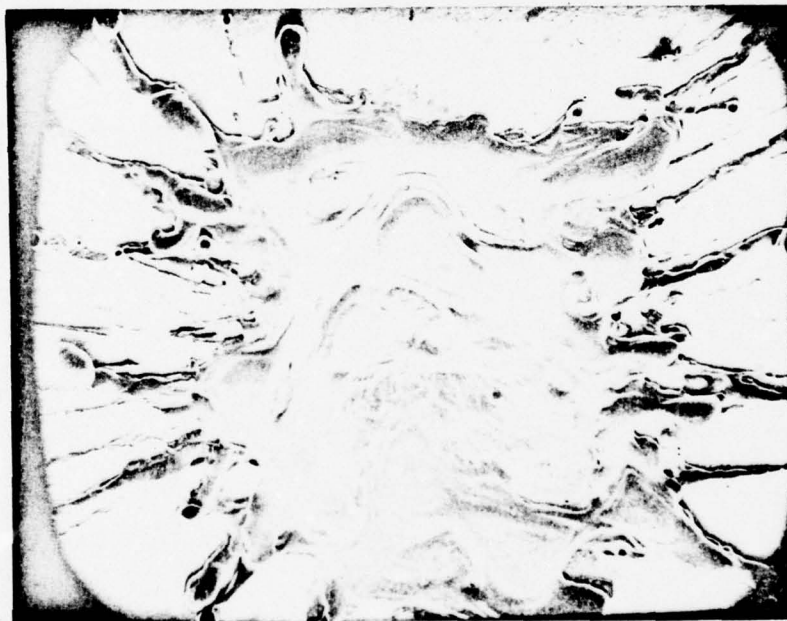
Region III. Region III is due to thermionic emission from the hot flushed metal and produces a positive target signal. The materials used in the verification were the thin oxides of Fe and Ni. Pictures of the target signal and the associated damage are shown in Figs. 19-22. From these figures one can see that Region III is more positive for those targets which have a larger amount of flushed metal.

9.3KV/20" (26Sep)



TARGET

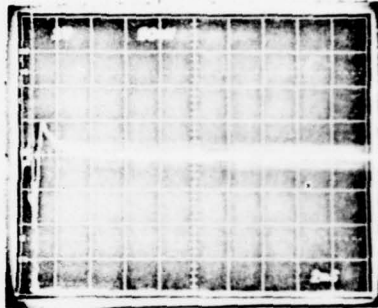
LASER



50X

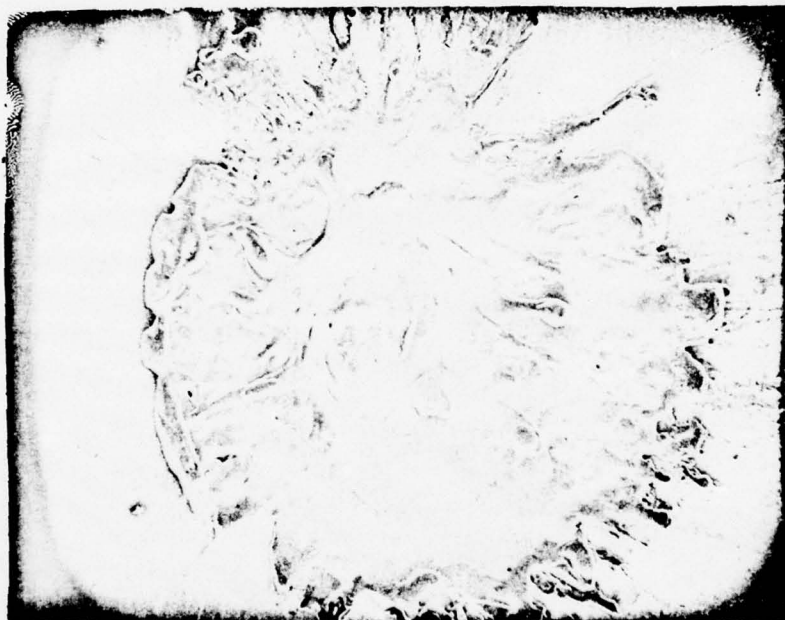
Fig. 19. Target signal and associated damage for thin oxide Fe.

10KV/40" (26Sep)



TARGET

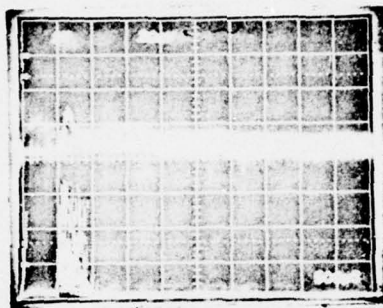
LASER



25X

Fig. 20. Target signal and associated damage for thin oxide Fe.

9.2KV/30"(26 Sep)



TARGET

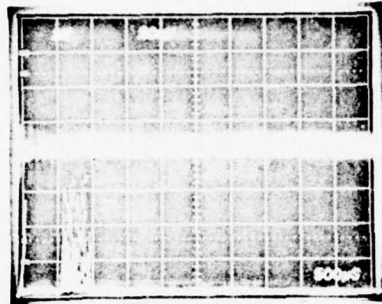
LASER



50X

Fig. 21. Target signal and associated damage for thin oxide Ni.

9.2KV/40" (26 Sep)



TARGET

LASER



50X

Fig. 22. Target signal and associated damage for thin oxide Ni.

Region IV. Region IV is due to an oxide tail formation which is brought about by the plume-surface interaction. This region is negative because negatively charged oxygen migrates to the surface and forms oxides. The downstream oxidation process begins with the plume-surface interaction. The factors which appear to influence the appearance of Region IV are the degree of coupling between the plume and surface, and the rate at which the oxides form. If there is sufficient coupling and the rate is sufficiently slow, then Region IV will appear as illustrated in Fig. 6. However, if either of these conditions is not fulfilled, then a distinct Region IV will not appear. The effect of the oxide formation will become lost in the preceeding region.

The only materials which had the fourth region were the cathode material and all forms of both cold-rolled steel and Fe (Fig. 23). The meaning of the target signal from the cathode material is not fully understood due to the limited amount of data collected. The reason for including the cathode material in this study is discussed in the next section.

Region IV was verified using clean cold-rolled steel. The approach used was to find an example where a relatively large oxide formed (Fig. 24(a) ) and an example where a minimum oxide formed (fig. 24(b) ). Figure 25 shows the oxide layer which has formed in Fig. 24(a).

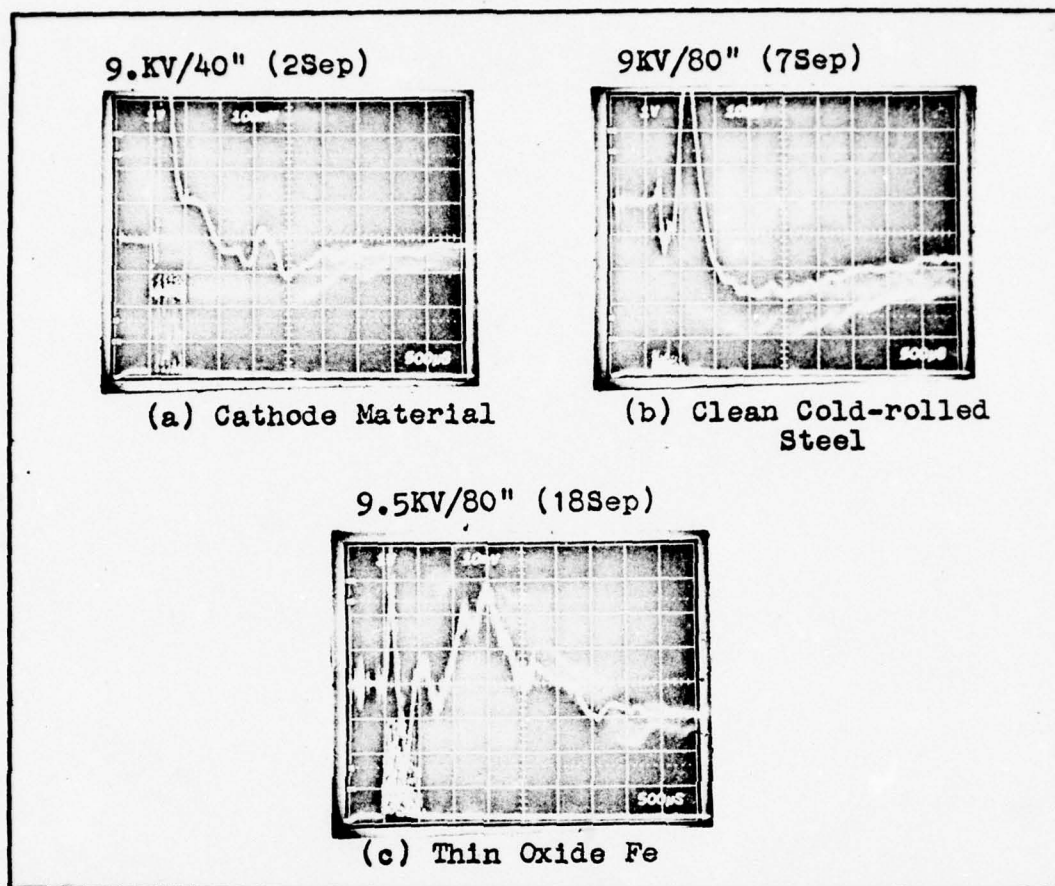


Fig. 23. Target signals for the cathode material, clean cold-rolled steel and thin oxide Fe.

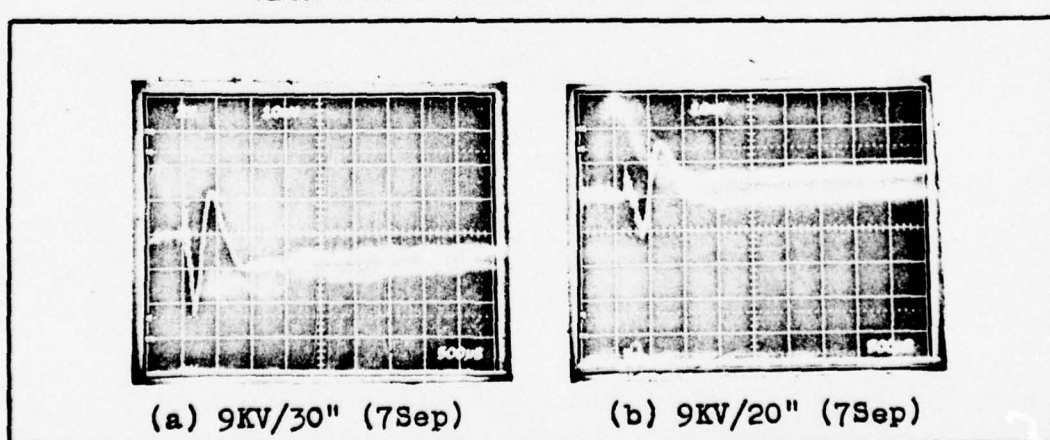


Fig. 24. Clean cold-rolled steel signals.

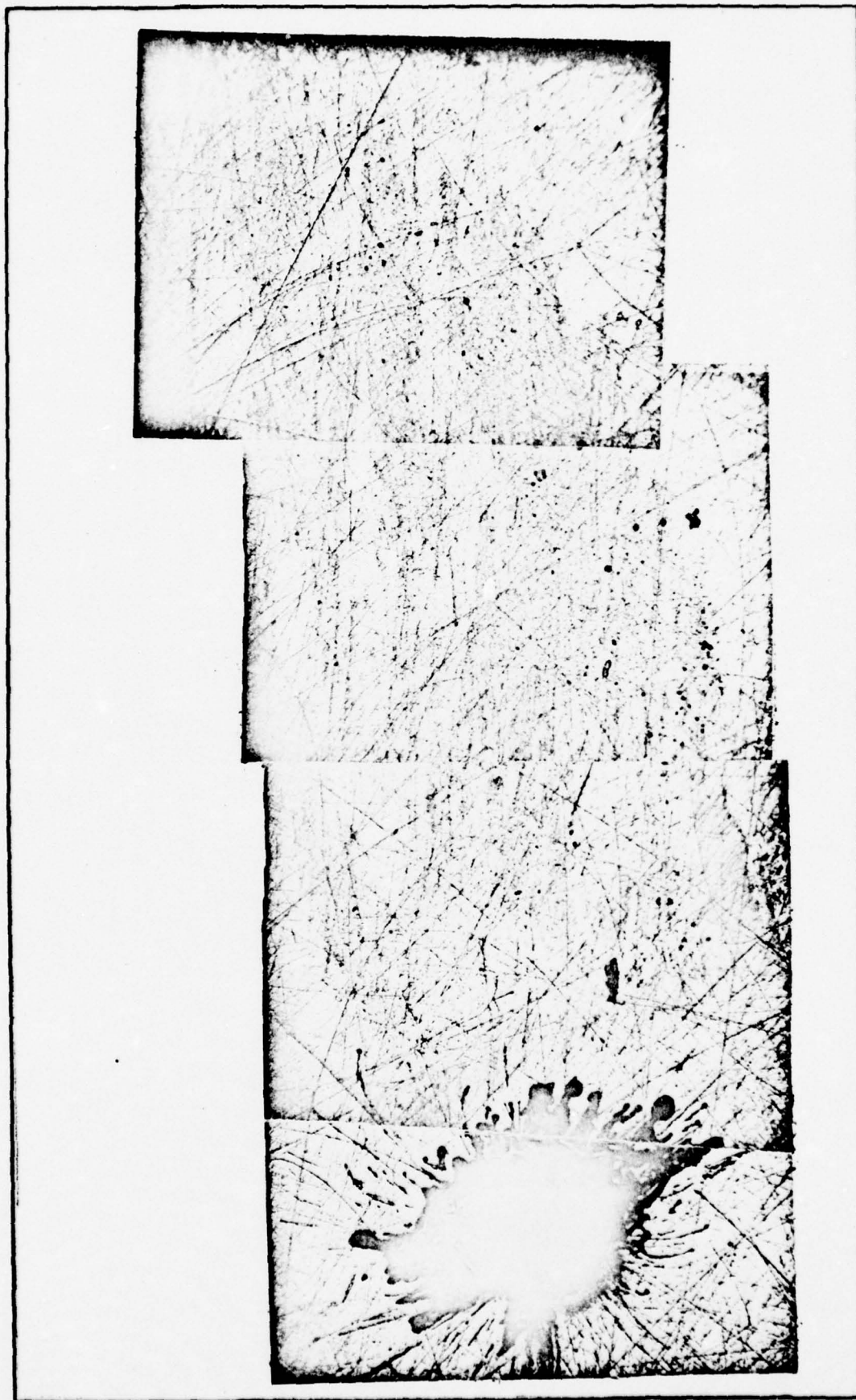


Fig. 25. Oxide layer for cold-rolled steel.

Columbium was a material which did not have the fourth region. However, based on a limited amount of notes regarding the observed relative intensities of the oxides formed, there appears to be a correlation between the oxide formed and the leading edge of Region III. This correlation is illustrated in Fig 26. Figure 27 shows the target signal.

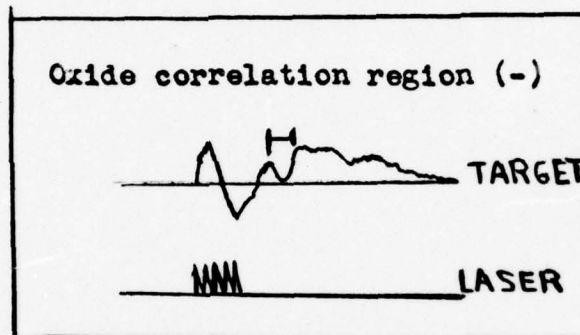


Fig. 26. Illustration of  
Fig. 27.

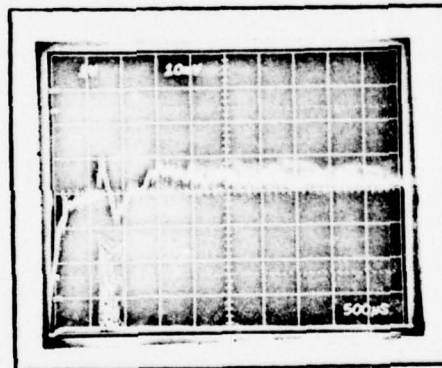


Fig. 27. Clean Cb target signal.

9KV/30" (11Sep)

Additional Experiments. When the experiments first began, it was noted that a loud noise, similar to the firing of a rifle could be heard when the laser was fired - this

noise is referred to as a "bang." Also, a large amount of molten metal was deposited on the window after each shot. When the sinusoidal target signal began to appear, it was noticed that the "bang" had decreased to a dull pop and the problem with the molten metal had disappeared. It was decided to visually observe the laser-target interaction in an attempt to understand what was happening. Unfortunately on the day this experiment was done, there was no film for the camera; therefore, the following is based on notes pertaining to cold-rolled steel targets.

The first experiment was to multiple fire the target at a given spot and observe the results. It was generally found that the first shot gave the loudest "bang" and ejected the least amount of molten metal. The light associated with the first shot was predominately white; however, it contained a small dot of blue light. After the first shot it was observed that the intensity of the blue light increased and the white light grew dimmer. Next, the signals were observed on an oscilloscope. For no airflow, the target signal looked like Fig. 28. However, for airflow

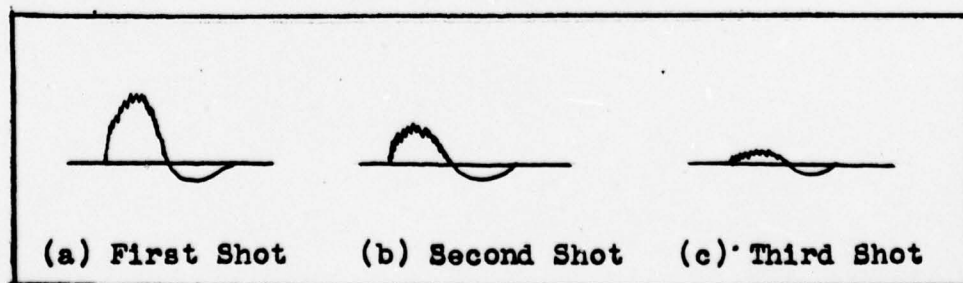


Fig. 28. Illustrative target signals for cold-rolled steel.

(6"Hg) the target signal looked like Fig. 29. These experi-

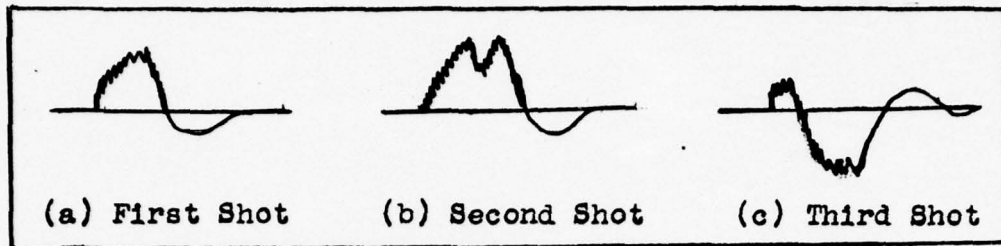


Fig. 29. Illustrative target signals  
for cold-rolled steel (6"Hg).

ments suggested (1) mass removal from the target might account for a decreased target signal, (2) plume-target coupling could account for the sinusoidal nature of the target signal, and (3) the "bang" was associated with poor coupling between the plume and the target.

The cathode material was cursorily examined to determine if a good thermionic emitter could cause the plume to decouple from the target in an airflow. This material produced a very loud "bang" and prevented any observable damage to the Ni base. No oxide tail was observed on the black surface of the cathode material and it is not known if the tail was absent or simply that the author could not see it. Therefore, the interpretation of the signal for the cathode material is questionable.

A clean Ni target was biased with +90V to obtain an order of magnitude estimate for the predicted value of the plume-hole coupling. The approach used was to estimate the electron density of the plume from the biased signal, and then use this density to estimate the un-biased target signal. Figure 30(a) shows the biased signal and 30(b) shows the

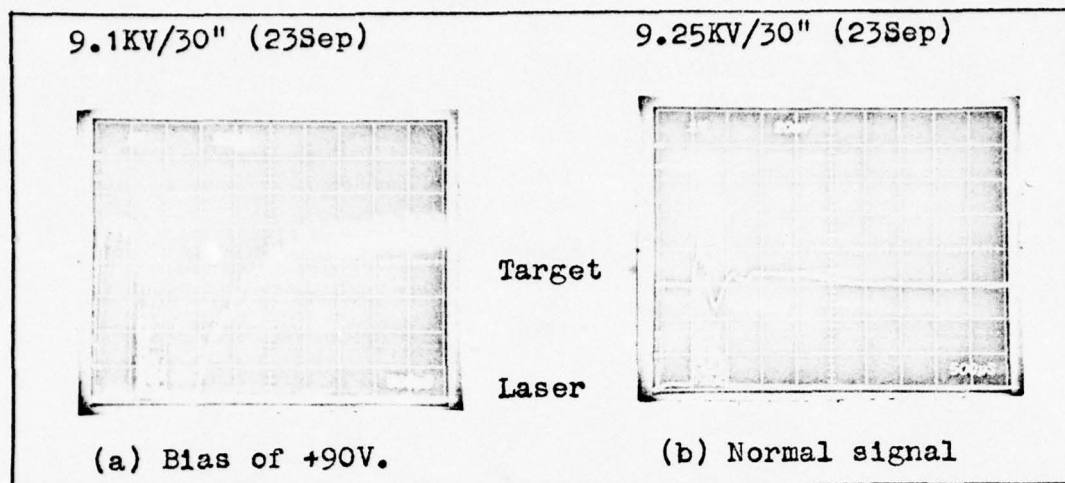


Fig. 30. Biased and un-biased target signal for clean Ni. normal signal. From Fig. 30(a), one can obtain a lower bound for the target current ( $I_{\min}$ ) by dividing the voltage (0.1V) by the scope impedance (1 Meg). Since the hole produced had a diameter of approximately 1.0mm, the flux ( $J_{\min}$ ) could be calculated by dividing  $I_{\min}$  by the area of the hole. The resulting value of  $J_{\min}$  is 0.127 amps/m<sup>2</sup>. The flux can also be written as:

$$J = ne\mu E \quad (1)$$

where  $n$  is the density of electrons,  $e$  is the charge of the electron,  $\mu$  is the electron mobility in air, and  $E$  is the electric field. The mobility in air is approximately  $5.0 \times 10^{-2}$  m<sup>2</sup>/v-sec. The value of  $E$  can be estimated by assuming that the surfaces of the target and stress chamber can be approximated as parallel plates. Therefore,

$$E = V/d \quad (2)$$

where  $d$  is the diameter of the tubing ( $3 \times 10^{-2} \text{ m}$ ) and  $V$  is the bias voltage (+90V). Substituting the value of  $E$  (3000 v/m) into Eq. 1 and solving for  $n$  yields

$$\begin{aligned} n_{\min} &= J_{\min} / [e \mu E] \\ &= (0.127 \text{ amps/m}^2) / [(1.6 \times 10^{-19} \text{ coul})(0.05 \text{ m}^2/\text{v-sec})(3000 \text{ v/m})] \\ &= 5.305 \times 10^{15} \text{ m}^{-3} \end{aligned} \quad (3)$$

The Debye length ( $\lambda_D$ ) can be calculated (Ref 12:71) using the equation

$$\lambda_D = \sqrt{(e_0 kT) / (e^2 n_{\min})} \quad (4)$$

For an assumed temperature of 2,000°K,  $\lambda_D^{\max}$  is  $4.243 \times 10^{-5} \text{ m}$ . This value is much smaller than the hole diameter ( $1.0 \times 10^{-3} \text{ m}$ ); therefore the first requirement ( $L \gg \lambda_D^{\max}$ ) for a plasma is fulfilled. The next requirement for a plasma is

$$n^{\min} (\lambda_D^{\max})^3 \gg 1 \quad (5)$$

The value of this product is 405; hence, a plasma exists and shielding effects occur. The potential associated with the sheath is of the order of a few  $kT$  - assume 5  $kT$  (Ref 16) to be specific. For a temperature of 2,000 K, 5  $kT$  is approximately equal to 1.0 ev. If it is assumed that this is the voltage which effectively acts on the plasma, then the average flux on the target is expressed by Eq. 1

$$J^{\min} = n^{\min} e \mu E \quad (1)$$

$$= n^{\min} \mu e V / d$$

$$= (5.305 \times 10^{15} \text{ m}^{-3}) (5 \times 10^{-2} \text{ m}^2/\text{v-sec}) (1.6 \times 10^{-19} \text{ J/eV}) (1 \text{ eV}) / 3 \times 10^{-2} \text{ m}$$

$$= 1.415 \times 10^{-3} \text{ amps/m}^2$$

The minimum un-biased voltage ( $V'$ ) is calculated by multiplying the above result by both the area of the 1.0 mm hole and the input impedance (1 Meg). The calculated value of  $V'$  is 1.11 mv, which favorably compares with the observed depth of Region II (Fig. 30(b)).

#### Simulated Jet Engine

The purpose of the simulator was to generate pockets so that the Positive Pocket Theory (Ref 1:6) could be experimentally verified. The simulator was composed of a stress chamber, particle separator, and Faraday Cage.

Pipe Signal. A six inch piece of copper tubing was inserted directly after the stress chamber, and was electrically isolated from the stress chamber and the tubing leading to the particle separator. The purpose of monitoring the pipe was to determine if any charging of the blow-off occurred between the stress chamber and the particle separator. If the pipe did not interact with the blow-off, then its average signal would be zero. The average value of the pipe signal (Fig. 31) was negative and implied that the blow-off material had been positively charged. This charging mechanism was

noted as a source of error since it was an uncontrollable parameter

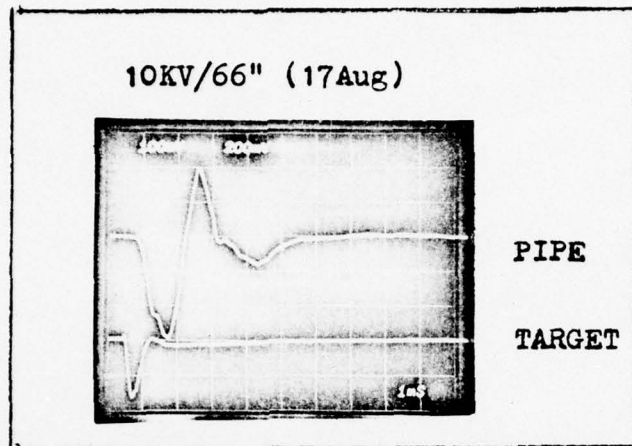


Fig. 31. Pipe signal for cold-rolled steel.

Particle Separator. The blow-off material had a net negative polarity and contained charged particles. The polarity of both the particles and the pocket could be obtained by examining the electrical signals from the particle separator. Figure 32 shows that blow-off from N1 contains negative particles and a positive pocket, and blow-off from T1 contains positive particles and a negative pocket. For example, Fig. 32(a) shows a positive box signal (200 mv scale) and a negative blade signal ( $\downarrow$ 200 mv scale); therefore, N1 blow-off contains negative particles.

Faraday Cage. The purpose of the Faraday Cage was to allow calculation of the net charge in the pocket and could be calculated with the aid of the integrator or directly from the Faraday Cage signal. With the exception of the cathode material and N1, blow-off from all materials contained negative pockets and positive particles. Nickel (Fig. 32(a) )

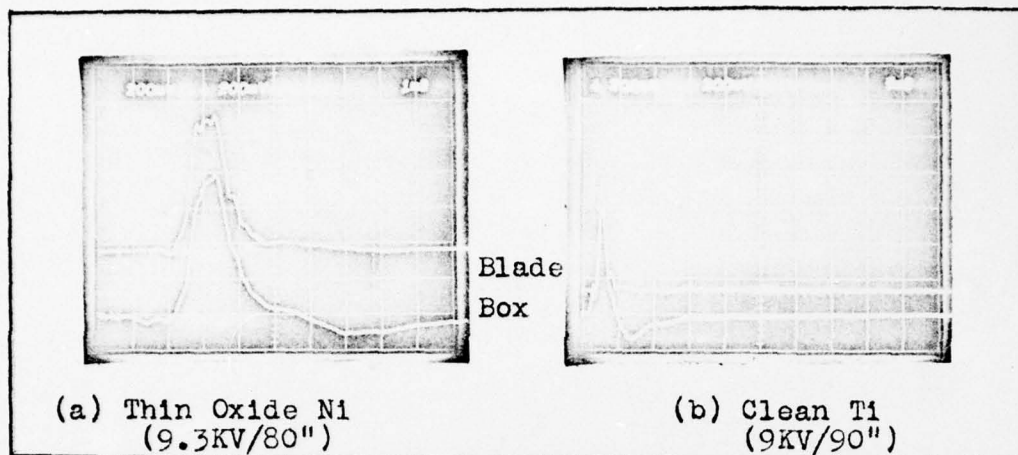


Fig. 32. Box and blade signals for N1 and T1.

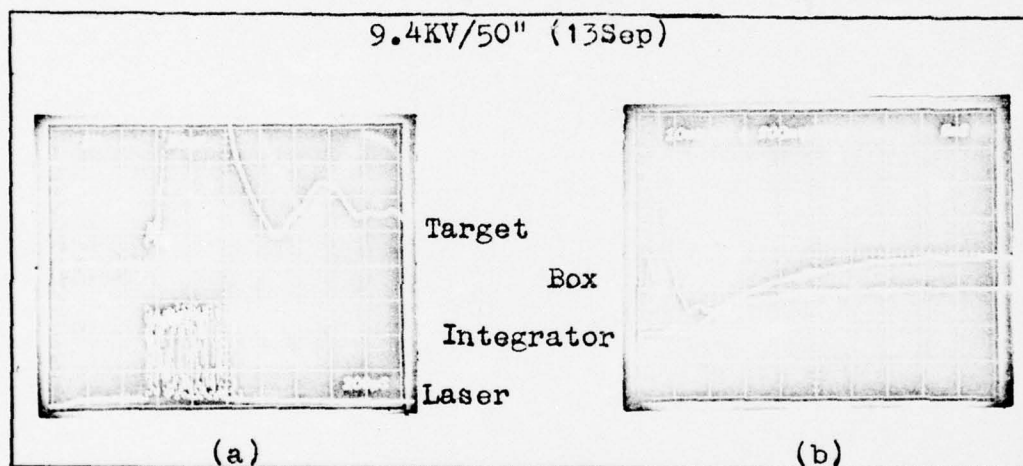


Fig. 33. Signals for thick oxide T1.

and the cathode material had positive pockets and negative particles. Figure 33(b) shows the box and integrator signals for thick oxide T1.

The oxidation process could generate a positive pocket (Fig. 34). To show this, the particle separator was removed and the target was irradiated with a laser beam which was focused about two centimeters in front of the target. This maximized the effects of oxidation and minimized the surface damage. Figure 34(b) shows that the blow-off has a net negative

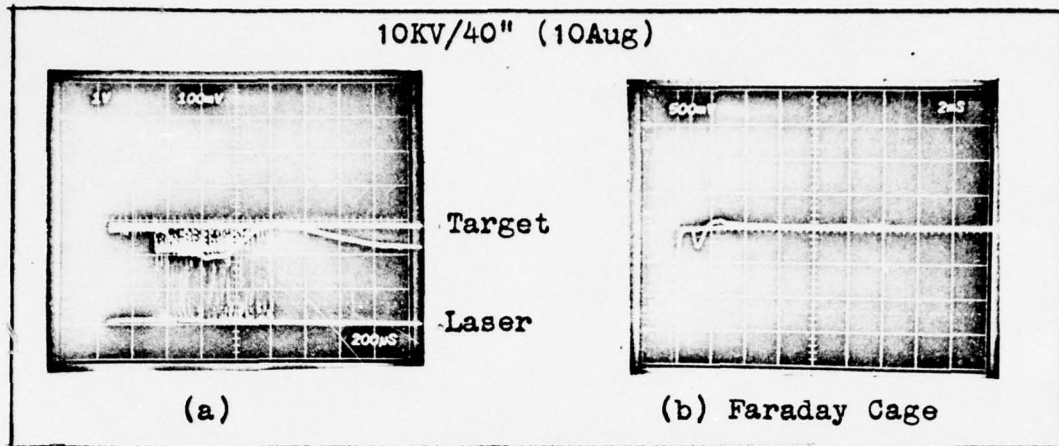


Fig. 34. Generation of positive  
pocket by oxidation.

charge for about 1.0 msec. Afterward, the net charge of the blow-off is positive and is due to oxidation of the target. When the target oxidizes, a net positive charge is left in the air stream, and it is this quantity which causes the Faraday Cage signal to go positive. This experiment plus the oxidation experiments performed by Mitchell (Ref 8) provides further support for the interpretation applied to Region IV.

#### IV. Results and Recommendations

##### Results

The results of this thesis are divided into two categories and are shown to be valid for laser fluxes less than  $4.8 \times 10^6$  watts per square centimeter and air speeds less than Mach 1.0. The first category pertains to the laser-target interaction and the second to the pockets generated.

Laser-Target. The electrical signal produced by a target which was irradiated by a pulsed ruby laser could be interpreted. With the possible exception of a cathode material, the interpretation was shown to be independent of the following target materials: cold-rolled steel, Fe, Ni, Ti, Ti 64, Cb, Mn, and Co. Furthermore, the shape of the target signal from all materials followed a reproducible pattern which had the general form of two cycles of a sine wave. Neglecting the cathode material, this form was divided into four regions and the interpretation applied to each region was as follows: (1) Region I - Laser induced thermionic emission, (2) Region II - Plume-target interaction, (3) Region III - Thermionic emission from the hot flushed material, and (4) Region IV - Oxide tail formation due to the plume-target interaction. The above results are based on correlations observed between the target signal and the observed target damage. The data base used to establish the above results consisted of approximately 1800 photographs. Of these, 950 photographs contain both the laser signal in conjunction with the target signal.

The interpretation applied to each region was verified by performing experiments designed to test the validity of the interpretation applied to each region.

Region I is due to laser induced thermionic emission which is critically dependent on surface contamination. The contamination purposely applied to the surface was a controlled oxide layer. The basis of the test was that the target signal should have a slope discontinuity when the laser began to interact with the material on which the oxide was grown. This discontinuity was experimentally observed. Furthermore, the position of the discontinuity with respect to the initial time the laser began to interact with the target had a strong correlation with the thickness of the oxide layer. That is a portion of the leading edge of the target signal allowed discrimination of targets having different oxide thicknesses.

The plume-target interaction is composed of a plume-hole interaction and a plume-surface interaction. The plume-hole interaction is a measure of the depth of the holes produced and was verified with no airflow - this minimized the plume-surface interaction. Targets were irradiated with the laser and the depth of the hole was compared with Region II. This comparison showed that deep holes had a more negative signal than shallow holes. Finally, a target was biased +90V and an order of magnitude analysis was used to predict the unbiased target signal of Region II. This value agreed with the experimental data and provided further support for

the interpretation given to the plume-hole interaction.

The plume-surface interaction was verified in an airflow. The basis of the verification was to show that the effect of plume could be maximized by tilting the target and minimized by irradiating the target on the downstream edge. These experiments were performed and above statements were shown to be true.

Region III was experimentally verified by comparing the amount of flushed material with the approximate area of this region. This comparison showed that large amounts of flushed material had larger areas than small amounts of flushed material. Photographs of the target and the corresponding target signal showing this correlation are presented in the Experiments section of this thesis.

Region IV only occurred with the cathode material and all forms of both cold-rolled steel and Fe. Cold-rolled steel was used in the verification. The procedure used to verify the interpretation consisted of providing an example where an oxide tail had formed and an example where it had not formed. Region IV was only present for the target which had the oxide tail. For those materials that did not have a Region IV, a limited amount of data tends to indicate that there is a correlation between a leading portion of Region III and the magnitude of the oxide formed. This possible correlation does not contradict the interpretations applied to Regions III and IV. It merely showed that possibly the oxidations rates are not slow enough to give rise to Region

IV. The material may oxidize so fast that its effects are only observable as a perturbation of the Region III signal.

Pockets. The blow-off material from the laser-target interaction was passed through a particle separator which removed charged metal particles. The resulting charged cloud, termed a pocket, then flowed through a section of stove pipe - this allowed the total charge of the pocket to be calculated. The particles separated from the blow-off and the resulting pocket always had opposite polarities. The purpose of generating pockets was to experimentally verify the Positive Pocket Theory proposed by Couch (Ref 1:6). The only materials in this study which produced positive pockets were Ni and a cathode material. The cathode material consisted of the carbonates of Ba, Sr, and Ni and were on a Ni base. Due to a problem with the laser, this study could not experimentally verify the Positive Pocket Theory; however, the experiments did substantiate it. This theory assumed pockets having a net charge of 10 to 100 nanocoloumb; however, the experiments were only able to generate pockets of the order of 1 nanocoloumb.

Positive pockets were also generated when a cold-rolled steel target was irradiated with a defocused laser beam. The defocused beam heated the surface and induced oxidation - this created a positive pocket. That is, the air stream was left with a net positive charge because of the negative charge transferred to the target in the oxidation process.

### Recommendations

It is recommended that the target signal (electrical) be monitored in all laser-target interaction to determine if a signature similar to the one presented in this thesis exists. This recommendation is particularly directed to the study of high energy lasers for the following two reasons. First, it may be possible to estimate the resulting target damage (the hole depth) by examining Region II of the target signal. The second reason pertains to plasma shielding. This technique could possibly be used in conjunction with other experiments to determine how well a plasma shields a target. It is also recommended that the relationship between the oxide thickness and the leading portion of the target signal be further investigated. It appears that the relationship offers the possibility of a quick and accurate method of determining oxide thickness. This technique should be applicable in any instance where dis-similar materials are used.

Finally, it is recommended that the electrostatic probe technique for predicting jet engine failures be supplemented with an equivalent of the Faraday Cage used in this experiment. The reason is that an engine component which is located near the exhaust would release a large number of particles when it began to fail. These particles could be detected by the particle detector. Internal components that fail further from the exhaust would produce few, if any, particles in the exhaust. This condition would be detected by the excess charge detector.

### Bibliography

1. Couch, R.P. The Use of Electrostatic Probes to Predict Jet Engine Failures. 1975 IEEE International Conference on Plasma Science, May 1975.
2. Vopalansky, R. Unpublished thesis. Wright-Patterson AFB, OH: Air Force Institute of Technology, December 1970.
3. Burgess, Ray W., Jr. An Investigation of the Detection of Charged Metal Particles in a Jet Engine Exhaust by a Cylindrical Electrostatic Probe. Wright-Patterson AFB, OH: Air Force Institute of Technology, June 1972, AD-745540.
4. Labo, J.A. The Theory of an Electrostatic Metal-Particle Sensor Operating in a Jet Engine Exhaust. Thesis, GEP/PH/73-13. Wright-Patterson AFB, OH: Air Force Institute of Technology, June 1973.
5. Couch, R.P. and R.C. Poch. An Ion Probe to Predict Failures in Jet Engines. 8th Annual FAA International Aviation Maintenance Symposium, November 1974.
6. Parker, L. Theory of an Electrostatic Probe in a Jet Exhaust. AFAL-TR-74-249. Wright-Patterson AFB, OH: Air Force Avionics Laboratory, September 1974.
7. Saj, M. et al. Evaluation of Experiments Using Electrostatic Probes to Detect Imminent Failure

- of Jet Engine Gas-Path Components. Contract #F33615-74-C-3091. Wright-Patterson AFB, OH: Air Force Flight Dynamics Laboratory, March 1975.
8. Mitchell, J. Exploring Wire Simulation of Jet-Engine Gas-Path Microdistresses. Thesis, GNE/PH/75D-5. Wright-Patterson AFB, OH: Air Force Institute of Technology, December 1975.
  9. Shapiro, A. The Dynamics and Thermodynamics of Compressible Fluid-Flow. Volume I, New York: The Ronald Press Company, 1953.
  10. Lichtman, D. and J. Ready. "Laser Beam Induced Emission." Physical Review Letters: 342-345, 15 April 1963.
  11. Gioro, F. et al. "Laser-Induced Thermionic Emission." Applied Physics Letters: 25-27, 15 July 1963.
  12. Seshadri, S. Fundamentals of Plasma Physics. New York: American Elsevier Publishing Co. Inc., 1973.
  13. Ready, J. Effects of High-Power Laser Radiation. Academic Press, New York, 1971.
  14. Per Kofstad. High-Temperature Oxidation of Metals. New York: John Wiley and Sons, Inc., 1966.
  15. Kittel, C. Elementary Solid State Physics. New York: John Wiley and Sons, Inc., 1962.
  16. Battle, E. and Couch, R. Curves for Reducing Collisionless-Cylindrical Langmuir Probe Data. AFB, OH: Air Force Institute of Technology, 1970.

## Appendix A

### Photographs

The purpose of this appendix is to present a sampling of the signals encountered in this study. Detailed notes on the physical appearance of the irradiated target are not presented. The reason is that once the meaning of a region was understood, notes were only recorded if either something unusual occurred or the interpretation of a region failed. Once the interpretation of the target signal was understood, the air supply became contaminated with oil. This precluded the possibility of obtaining detailed notes, including photographs of the target damage, so that the interpretation of the regions could be checked for each material examined.

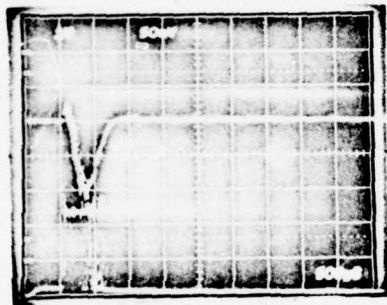
Before proceeding, one should remember that the photographs contain two voltage scales. The scale on the left refers to the bottom trace and the scale on the right refers to the top trace. Furthermore, an arrow ( $\downarrow$ ) means that the polarity of that scale has been inverted. Finally, it should be remembered that the integrator reversed the polarity of the signal.

COLD-ROLLED STEEL

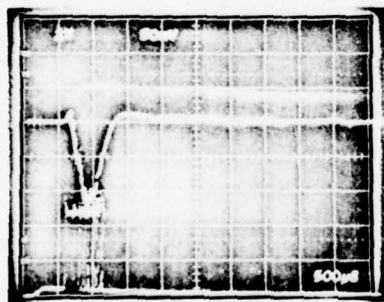
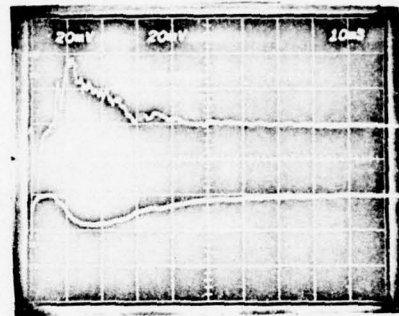
(7 Sep)

Target  
Detector

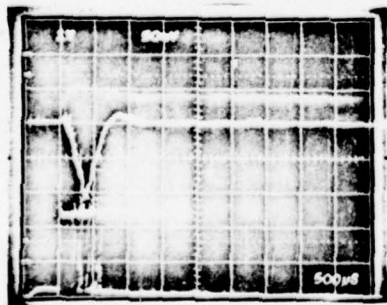
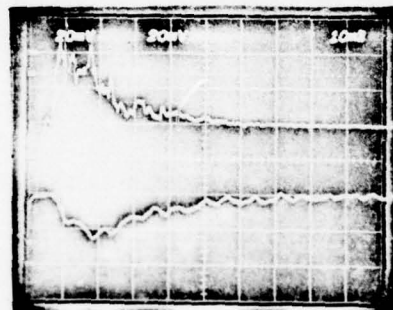
Box + Blade  
Faraday Cage



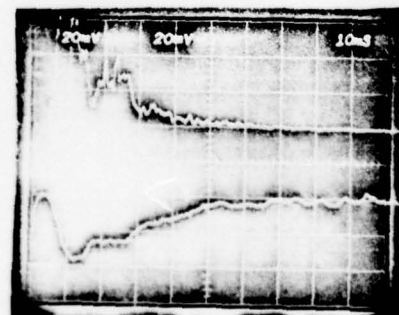
9.5KV/10"



9.5KV/30"



9.5KV/50"

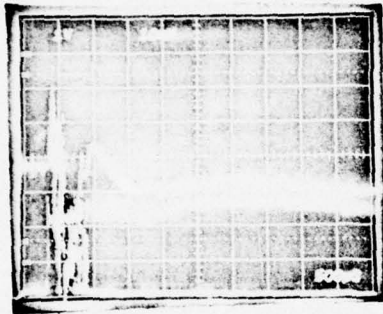


CLEAN COLD-ROLLED STEEL

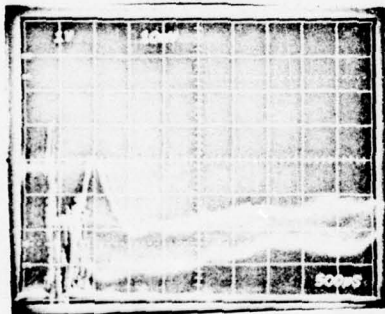
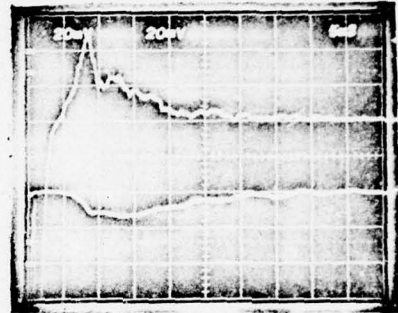
(12 Sep)

Target  
Detector

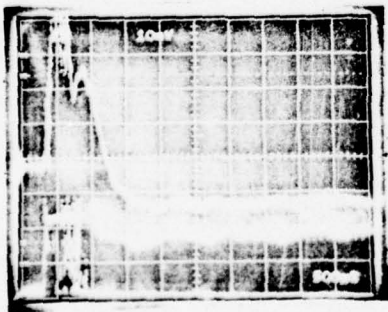
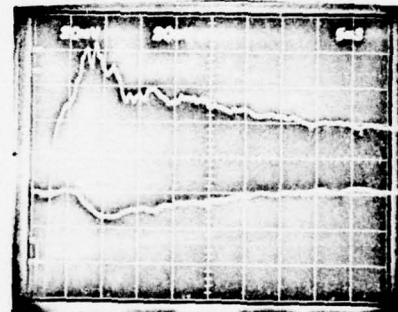
Box + Blade  
Faraday Cage



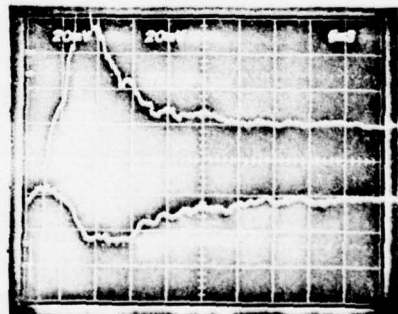
9.5KV/20"



9.5KV/30"



9.5KV/50"



CLEAN Fe

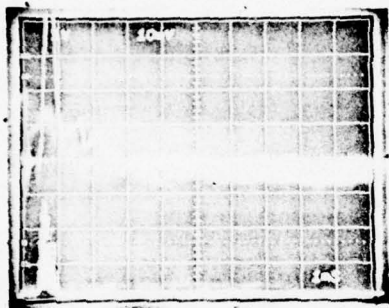
(18 Sep)

Target

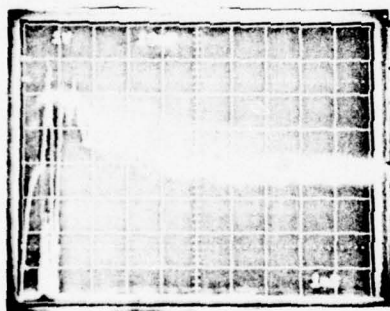
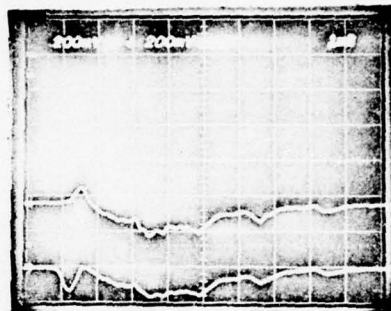
Blade

Detector

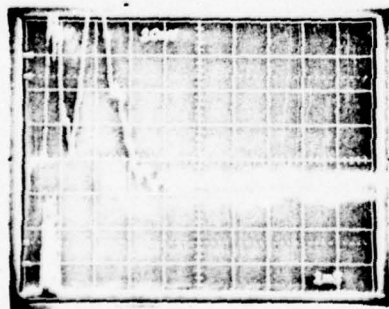
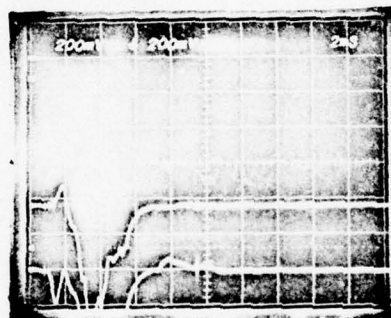
Box



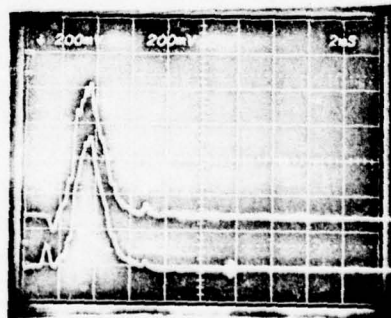
9.3KV/40"



9.5KV/70"



9.5KV/80"



THIN OXIDE Fe

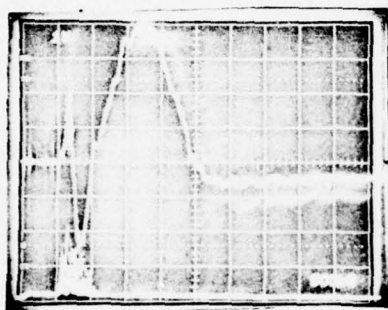
(18 Sep)

Target

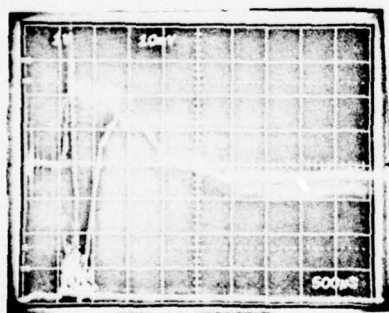
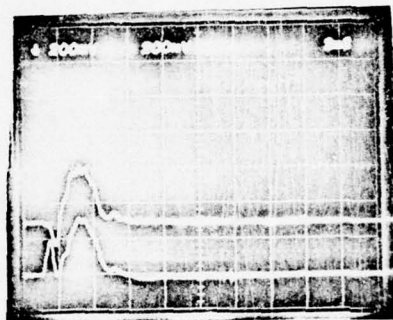
Blade

Detector

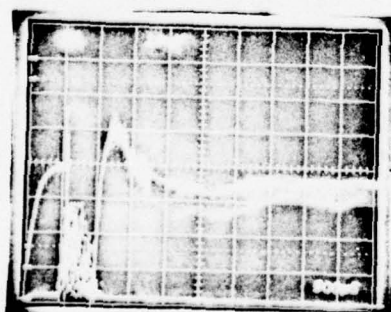
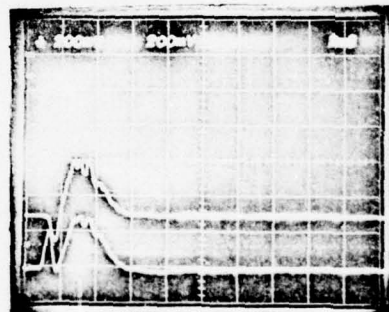
Box



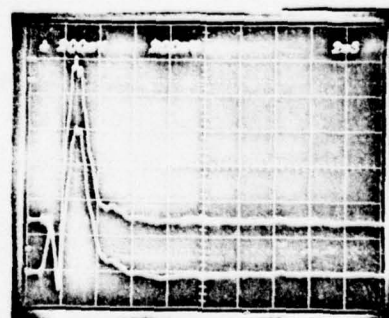
9.3KV/40"



9.3KV/80"



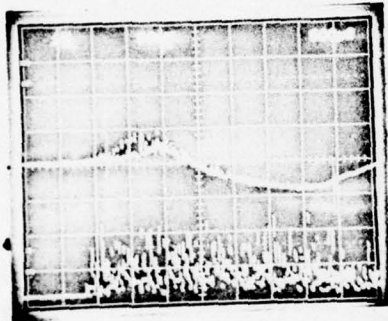
9.5KV/40"



THICK OXIDE Fe

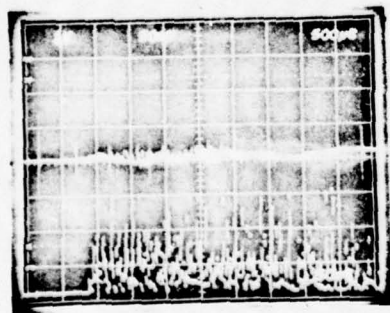
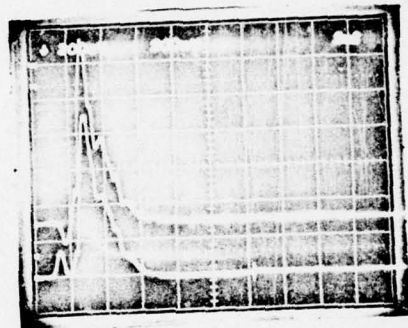
(18 Sep)

Target  
Detector

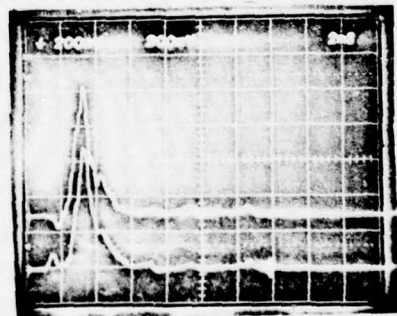


9.4Kv/80"

Blade  
Box



9.4KV/80"

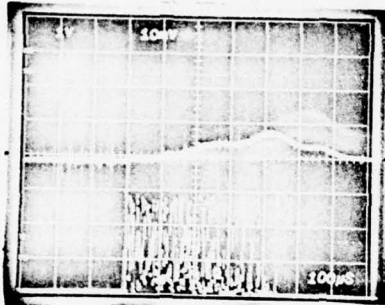


POLISHED N1

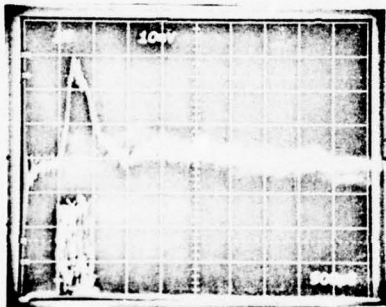
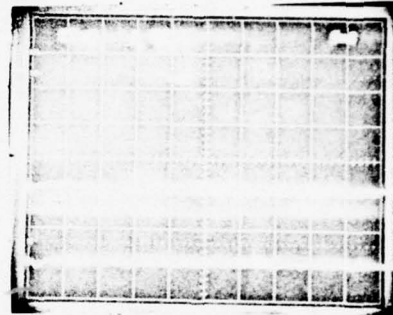
(19 Sep)

Target  
Detector

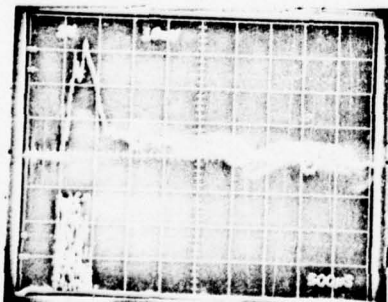
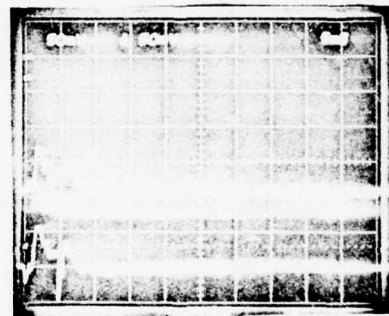
Blade  
Box



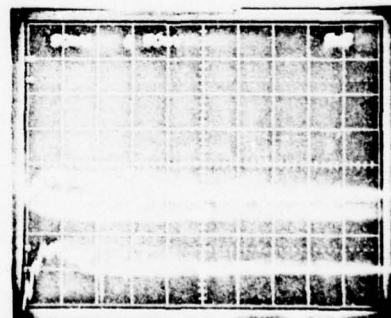
9KV/40"



9.5KV/80"



9.5KV/80"

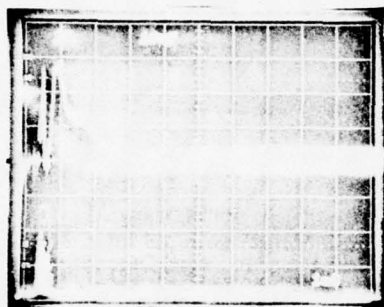


CLEAN N1

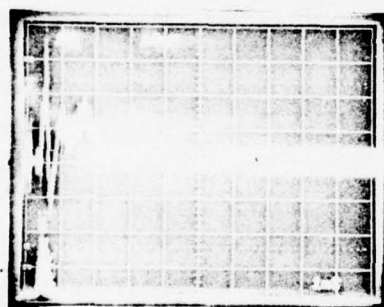
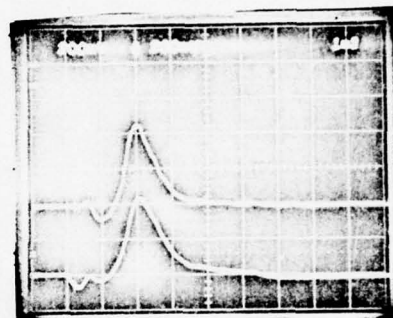
(18 Sep)

Target  
Detector

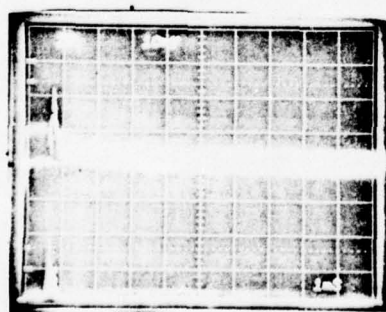
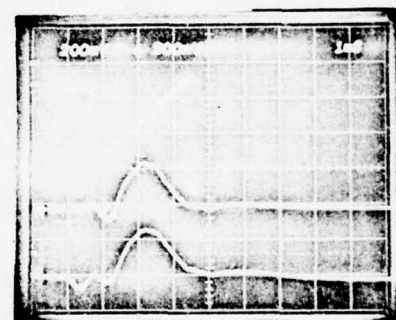
Blade  
Box



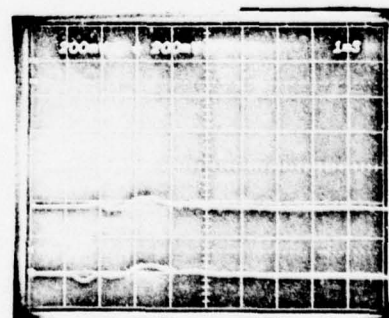
9.3KV/30"



9.3KV/30"



9.3KV/30"

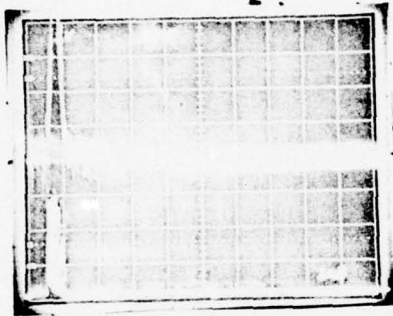


THIN OXIDE N1

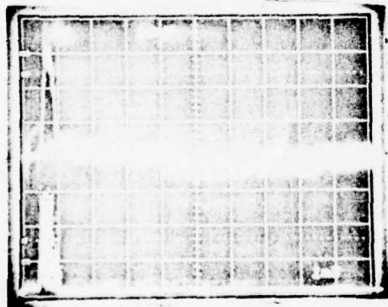
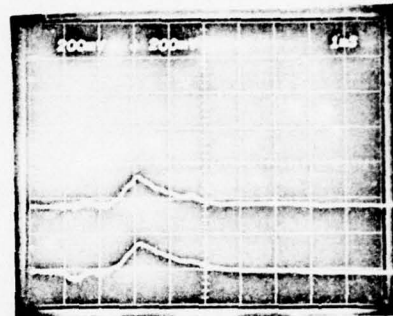
(18 Sep)

Target  
Detector

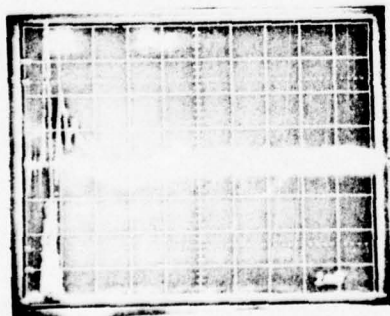
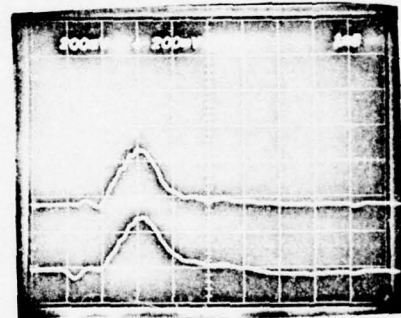
Blade  
Box



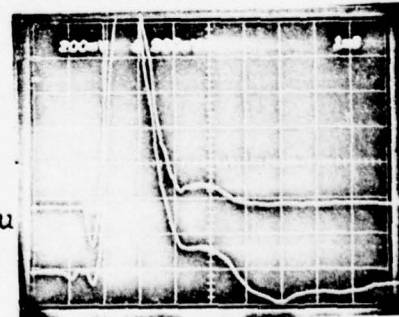
9.3KV/40"



9.5KV/30"



9.5KV/80"  
punched thru

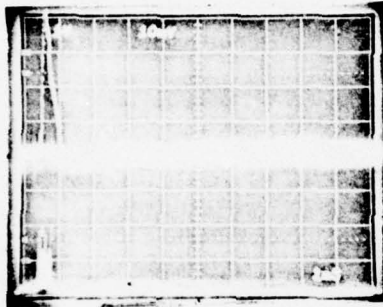


THICK OXIDE N1

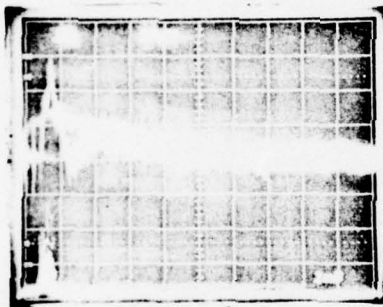
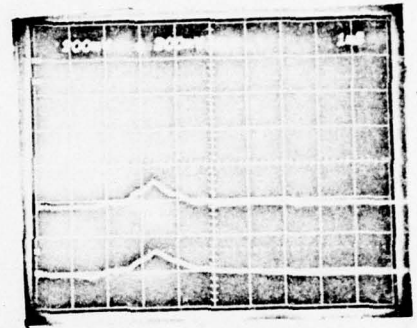
(18 Sep)

Target  
Detector

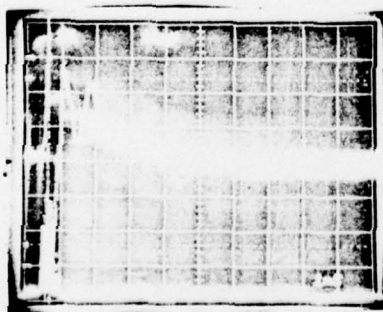
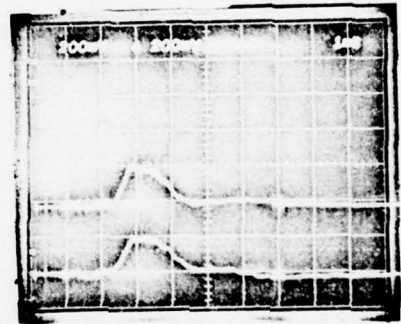
Blade  
Box



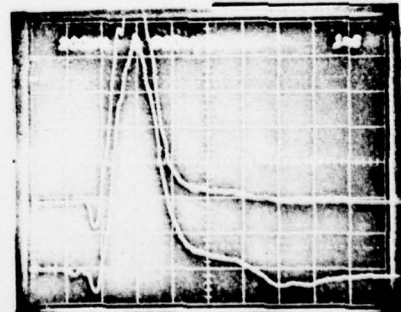
9.3KV/40"



9.3KV/80"



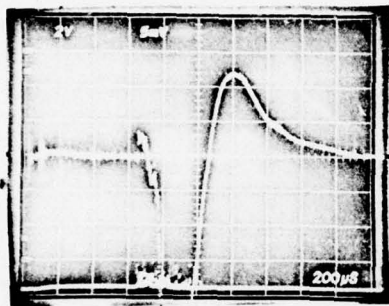
9.4KV/80"  
punched thru



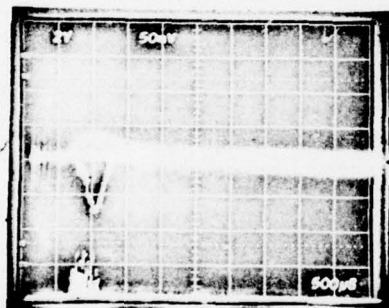
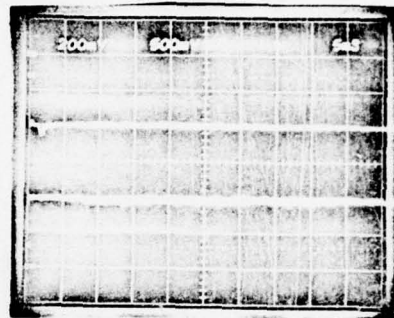
T1 64  
(28 July)

Target  
Detector

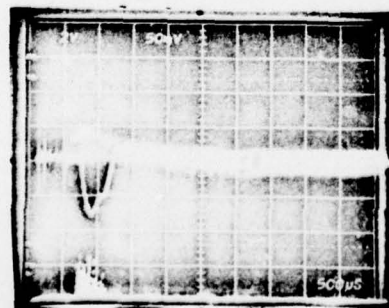
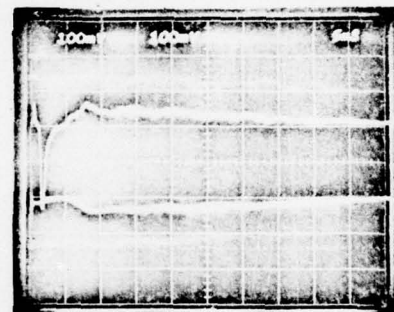
Box + Blade  
Faraday Cage



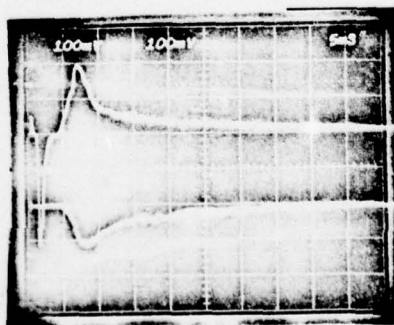
9KV.30"



9KV/30"



9KV/50"

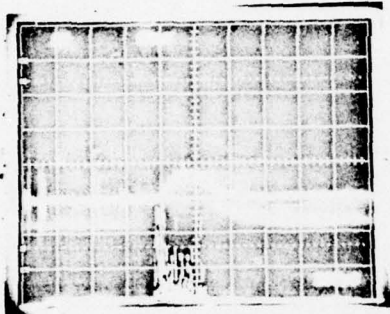


CLEAN T1

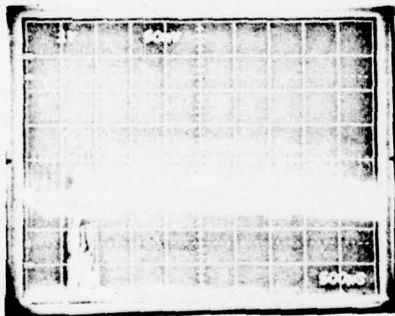
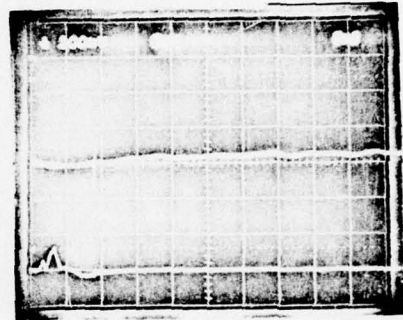
(13 Sep)

Target  
Detector

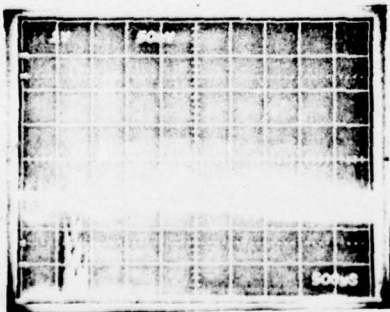
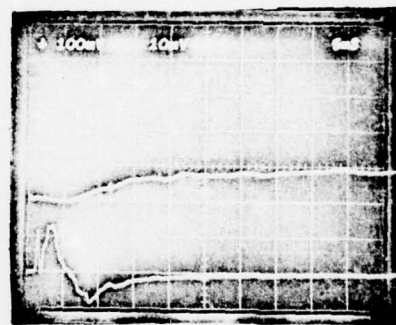
Integrator  
Box



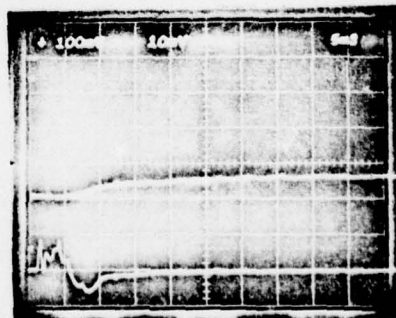
9KV/30"



9KV/40"



9KV/50"

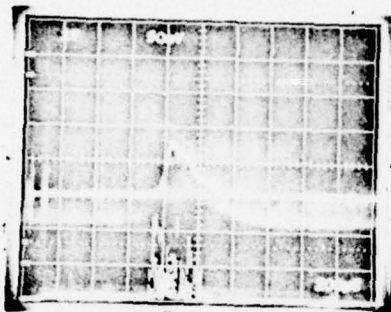


THIN OXIDE T1

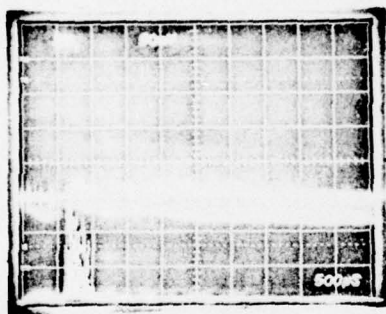
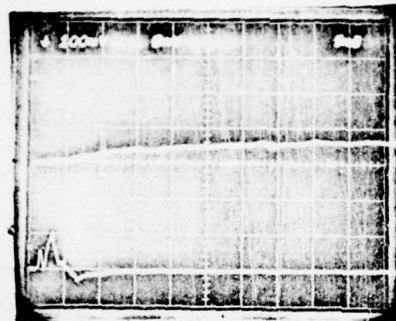
(13 Sep)

Target  
Detector

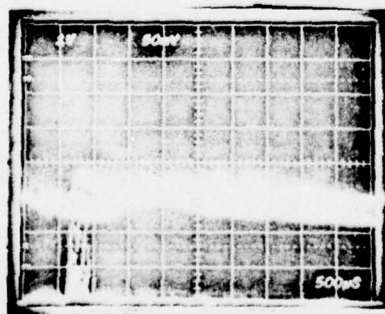
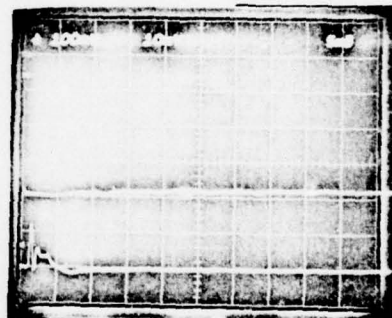
Integrator  
Box



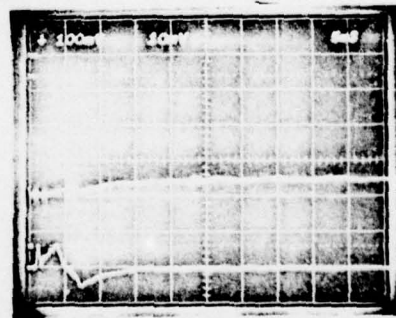
9KV/30"



9KV/40"



9KV/50"

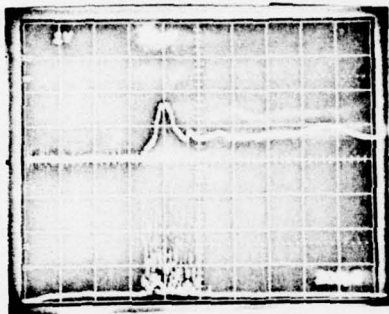


THICK OXIDE T1

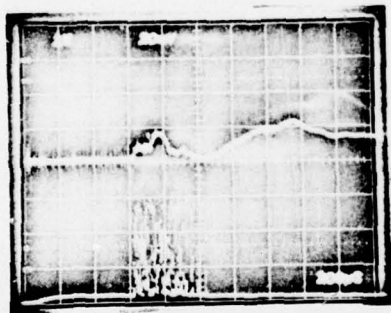
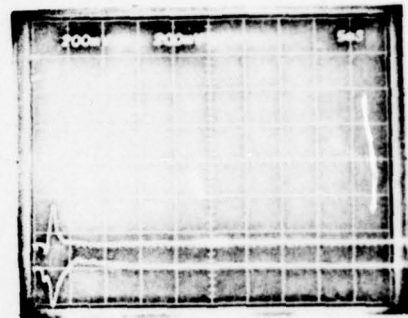
(12 Sep)

Target  
Detector

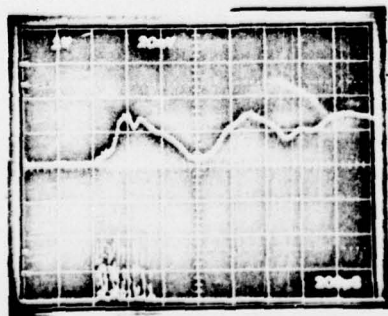
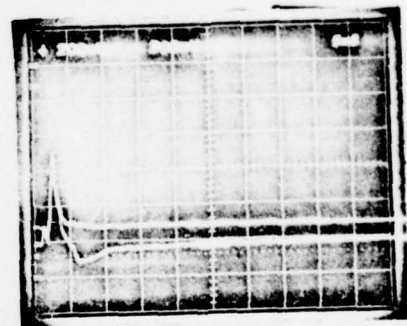
Blade  
Box



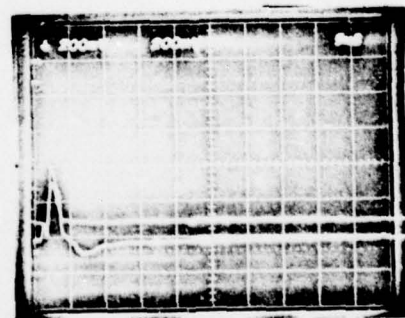
9KV/40"



9KV/40"



9KV/90"



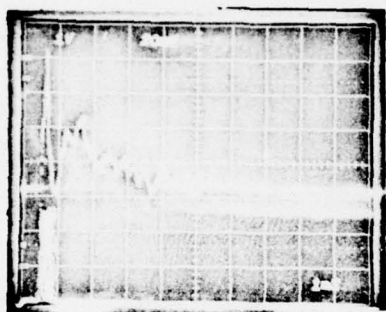
CLEAN Cb

(11 Sep)

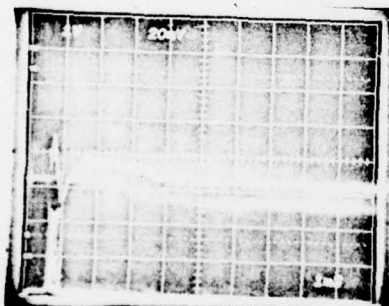
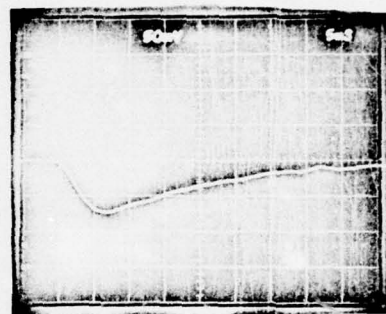
Target

Faraday Cage

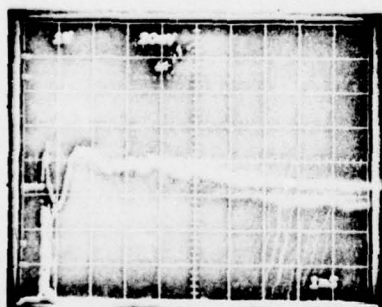
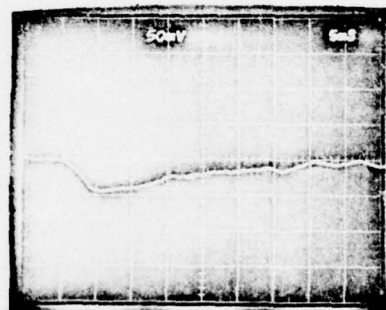
Detector



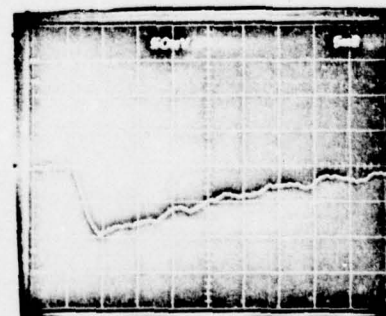
9.25KV/30"



9.25KV/40"



9.25KV/50"

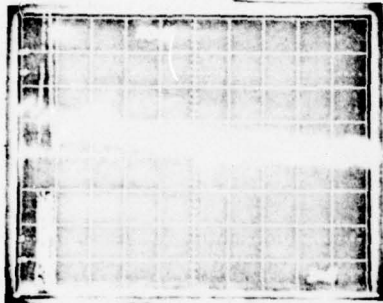


THIN OXIDE Cb

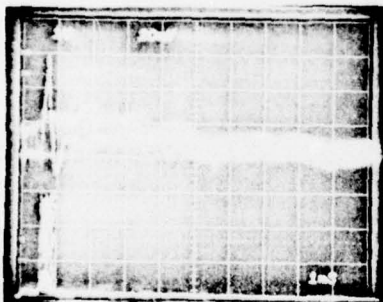
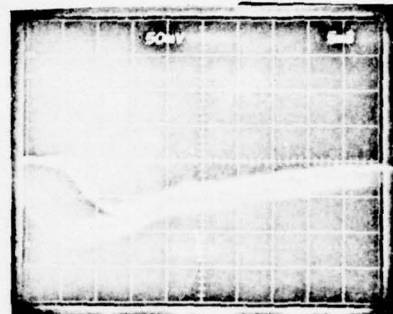
(13 Sep)

Target  
Detector

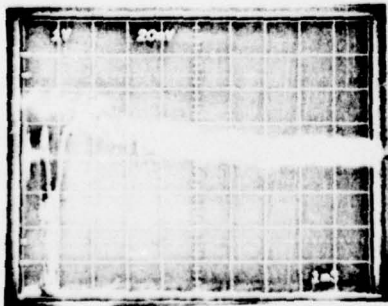
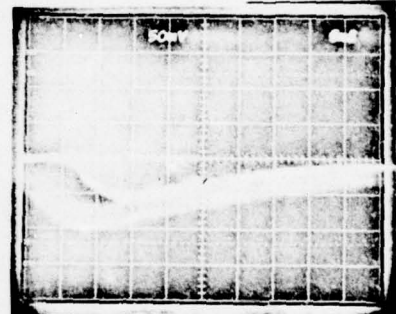
Faraday Cage



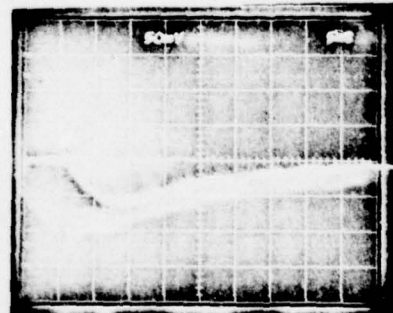
9.25KV/30"



9.25KV/40"

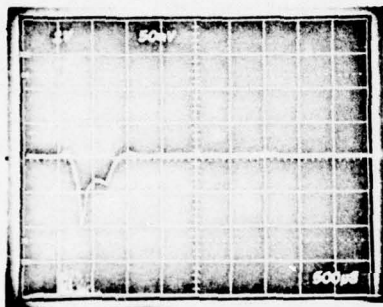


9.25KV/50"



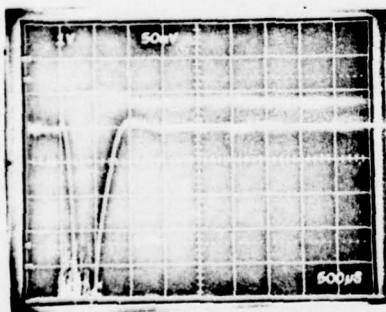
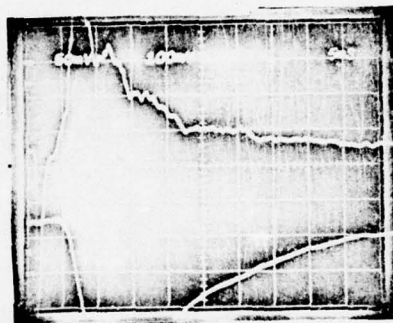
Ge  
(2 Sep)

Target  
Detector

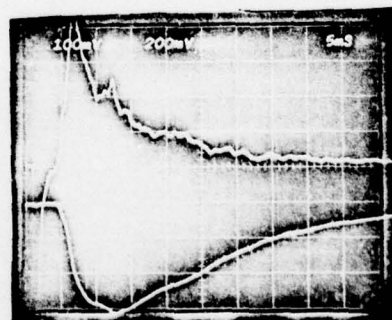


9.5KV/40"

Box + Blade  
Faraday Cage



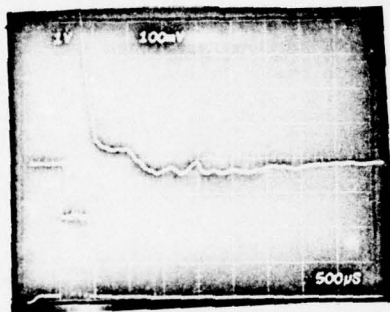
9.75KV/40"



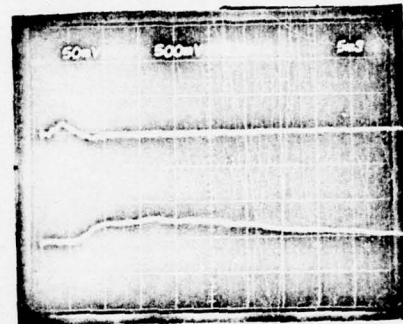
CATHODE MATERIAL

(2 Sep)

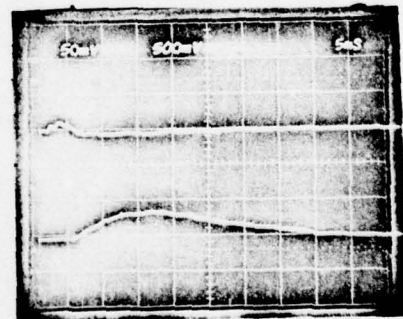
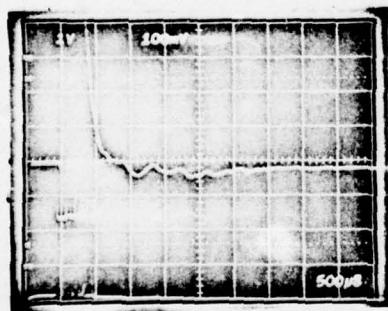
Target  
Detector



Box + Blade  
Faraday Cage



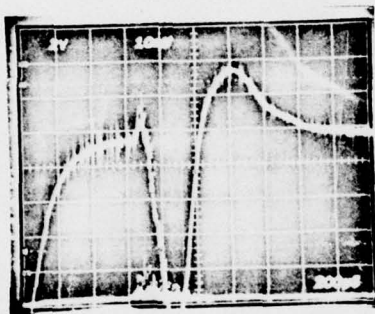
9.5KV/40"



9.5KV/40"

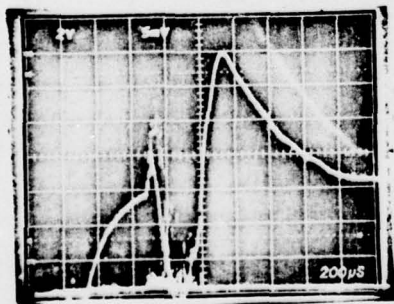
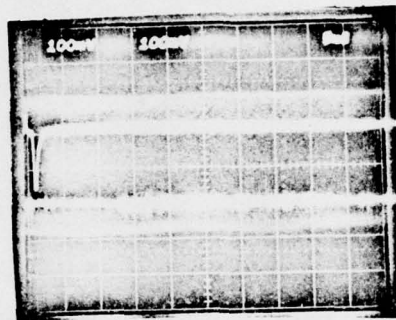
COBALT  
(28 July)

Target  
Detector



9KV/30"

Box + Blade  
Faraday Cage

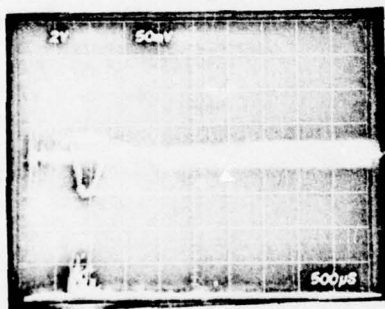


9KV/30"

overexposed

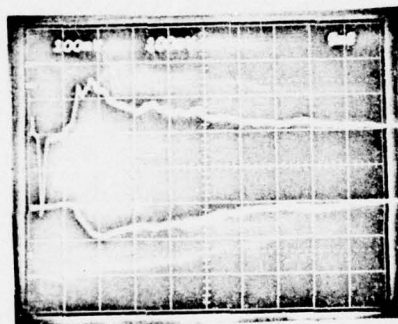
Mn  
(28 July)

Target  
Detector



9KV/30"

Box + Blade  
Faraday Cage



### Vita

Richard D. Arlen Jr.s' first duty station was Rome Air Development Center. He served as a Project Engineer in the field of laser optics. During this assignment he attended Squadron Officers' School at Maxwell Air Force Base. He was next assigned to the Pentagon with an assigned duty station at Headquarters Bureau of Narcotics and Dangerous Drugs (BNDD). While there, he served as Program Manager for a joint USAF/BNDD project. Following a short tour at the Air Force Avionics Lab, he entered the Air Force Institute of Technology School of Engineering to pursue a Master of Science Degree.

Permanent address: 6819 Moss Rose  
Houston, Texas 77017

Unclassified

SECURITY CLASSIFICATION OF THIS PAGE (When Data Entered)

REPORT DOCUMENTATION PAGE		READ INSTRUCTIONS BEFORE COMPLETING FORM
1. REPORT NUMBER AFIT/GEP/PH/75D-14	2. GOVT ACCESSION NO. <i>Master's thesis</i>	3. RECIPIENT'S CATALOG NUMBER
4. TITLE (and Subtitle) AN INVESTIGATION OF LASER-TARGET INTERACTION SIGNALS	5. TYPE OF REPORT & PERIOD COVERED MS Thesis	
7. AUTHOR(s) Richard D. Arlen, Jr Captain USAF	6. PERFORMING ORG. REPORT NUMBER	
9. PERFORMING ORGANIZATION NAME AND ADDRESS AFIT-EN	8. CONTRACT OR GRANT NUMBER(s)	
11. CONTROLLING OFFICE NAME AND ADDRESS AFFDL	10. PROGRAM ELEMENT, PROJECT, TASK AREA & WORK UNIT NUMBERS	
14. MONITORING AGENCY NAME & ADDRESS (if different from Controlling Office)	12. REPORT DATE <i>11</i> Dec 75	
	13. NUMBER OF PAGES 82 <i>(12) 85 p.</i>	
	15. SECURITY CLASS. (of this report) Unclassified	
15a. DECLASSIFICATION/DOWNGRADING SCHEDULE		
16. DISTRIBUTION STATEMENT (of this Report) Approved for public release; distribution unlimited		
17. DISTRIBUTION STATEMENT (of the abstract entered in Block 20, if different from Report)		
18. SUPPLEMENTARY NOTES APPROVED FOR PUBLIC RELEASE IAW AFR 190-17.  JERRAL F. GUESS, Capt, USAF Director of Information		
19. KEY WORDS (Continue on reverse side if necessary and identify by block number) Laser damage Electron emission Plume-target interaction Jet engine failure simulator		
20. ABSTRACT (Continue on reverse side if necessary and identify by block number) 400,000 Micro distresses were created in a simulated jet engine using a pulsed ruby laser, and the electrical signals were studied at various points in the simulator. Average power levels of the target ranged from $4.0 \times 10^5$ to $4.77 \times 10^6$ watts per square centimeter. Target materials investigated were cold-rolled steel, Ti 64, Mn, Co, a cathode material, and high purity Fe, Ni, Ti, and Cb. It was found that the target signals have a reproductive pattern. The most general pattern observed could be separated into four $\rightarrow$ 400,000		

DD FORM 1 JAN 73 1473

EDITION OF 1 NOV 65 IS OBSOLETE

UNCLASSIFIED

SECURITY CLASSIFICATION OF THIS PAGE (When Data Entered)

*012225*

Unclassified

SECURITY CLASSIFICATION OF THIS PAGE (When Data Entered)

regions and had the general appearance of two cycles of a sine wave. With the possible exception of the cathode material, the interpretation applied to each region was independent of the target material used. The interpretation applied to each region is: Region I - laser induced thermionic emission, Region ~~II~~ - plume-target interaction, Region ~~III~~ - thermionic emission of the hot flushed material, and Region ~~IV~~ - oxide tail formation due to the plume-target interaction. A leading portion of Region I correlated with the thickness of the oxide layer on the target, and in the absence of airflow, Region ~~II~~ correlated with the depth of the hole. It was found that the blow-off from the cathode material and Ni had negative particles and produced positive pockets upon passage through the simulator. The simulator basically removed charged particles from the air stream. All other materials produced positive particles and negative pockets. It was also found that oxidation produced positive pockets. These experiments substantiate the Positive Pocket Theory proposed by Couch and suggest expanding it to include negative pockets.

